A&A 506, 303–319 (2009)
DOI: 10.1051/0004-6361/200913096

Astronomy & Astrophysics
Special feature

The CoRoT space mission: early results

The CoRoT-7 planetary system: two orbiting super-Earths⋆,⋆⋆

D. Queloz[1], F. Bouchy[2,3], C. Moutou[4], A. Hatzes[5], G. Hébrard[2], R. Alonso[1], M. Auvergne[6], A. Baglin[6], M. Barbieri[4], P. Barge[4], W. Benz[7], P. Bordé[8], H. J. Deeg[9], M. Deleuil[4], R. Dvorak[10], A. Erikson[11], S. Ferraz Mello[12], M. Fridlund[13], D. Gandolfi[5], M. Gillon[1,14], E. Guenther[5], T. Guillot[15], L. Jorda[4], M. Hartmann[5], H. Lammer[16], A. Léger[8], A. Llebaria[4], C. Lovis[1], P. Magain[14], M. Mayor[1], T. Mazeh[17], M. Ollivier[8], M. Pätzold[18], F. Pepe[1], H. Rauer[11,19], D. Rouan[6], J. Schneider[20], D. Segransan[1], S. Udry[1], and G. Wuchterl[5]

(Affiliations can be found after the references)

Received 8 August 2009 / Accepted 26 August 2009

ABSTRACT

We report on an intensive observational campaign carried out with HARPS at the 3.6 m telescope at La Silla on the star CoRoT-7. Additional simultaneous photometric measurements carried out with the Euler Swiss telescope have demonstrated that the observed radial velocity variations are dominated by rotational modulation from cool spots on the stellar surface. Several approaches were used to extract the radial velocity signal of the planet(s) from the stellar activity signal. First, a simple pre-whitening procedure was employed to find and subsequently remove periodic signals from the complex frequency structure of the radial velocity data. The dominant frequency in the power spectrum was found at 23 days, which corresponds to the rotation period of CoRoT-7. The 0.8535 day period of CoRoT-7b planetary candidate was detected with an amplitude of 3.3 m s^{-1}. Most other frequencies, some with amplitudes larger than the CoRoT-7b signal, are most likely associated with activity. A second approach used harmonic decomposition of the rotational period and up to the first three harmonics to filter out the activity signal from radial velocity variations caused by orbiting planets. After correcting the radial velocity data for activity, two periodic signals are detected: the CoRoT-7b transit period and a second one with a period of 3.69 days and an amplitude of 4 m s^{-1}. This second signal was also found in the pre-whitening analysis. We attribute the second signal to a second, more remote planet CoRoT-7c . The orbital solution of both planets is compatible with circular orbits. The mass of CoRoT-7b is 4.8 ± 0.8 ($M_\oplus$) and that of CoRoT-7c is 8.4 ± 0.9 ($M_\oplus$), assuming both planets are on coplanar orbits. We also investigated the false positive scenario of a blend by a faint stellar binary, and this may be rejected by the stability of the bisector on a nightly scale. According to their masses both planets belong to the super-Earth planet category. The average density of CoRoT-7b is $\rho = 5.6 \pm 1.3$ g cm^{-3}, similar to the Earth. The CoRoT-7 planetary system provides us with the first insight into the physical nature of short period super-Earth planets recently detected by radial velocity surveys. These planets may be denser than Neptune and therefore likely made of rocks like the Earth, or a mix of water ice and rocks.

Key words. stars: planetary systems – techniques: radial velocities – techniques: photometric – stars: activity – stars: starspots

1. Introduction

For the past several years transit searches have experienced considerable success at discovering new extra-solar planets (planets orbiting stars other than the Sun). Among the long list of extra-solar planets, more than 50 have been found transiting their host stars. While transiting systems represent only a small fraction of the known planetary systems, they are particularly important because the special transit geometry strongly constrains the orbital inclination of the planets and allows their masses and radii to be derived. The mass-radius relation for exoplanets allows us to probe their internal structure, a key element in their formation and evolution. In practice, the physical size of a transiting planet is derived directly, with the period of the transiting body and the mean density of the star, from the analysis of the light curve. This former parameter, combined with the stellar effective temperature, may be compared with stellar evolution models to retrieve both the mass and the radius of the star, and thus the precise radius of the planet (Mazeh et al. 2000; Hebb et al. 2009).

For all transit search programs, either from the ground or from space, follow-up observation campaigns are needed to establish the planetary origin of the transit signal. The goal of these additional programmes is to remove ambiguities in the nature of the transiting object and to derive the planet mean density needed for insights into the planet structure. Some of the transiting *candidates* initially identified from their transit light curves turn out to be a special configuration of an unresolved fainter, eclipsing stellar system (Torres et al. 2004). Required observations usually include ground based photometry (Deeg et al. 2009), spectroscopy, and above all precise radial velocity measurements (Bouchy & Queloz 2007).

The CoRoT space telescope, launched in December 2006, observes two different fields every year for 150 uninterrupted days (respectively towards the direction of the anticenter and the center of the Galaxy). Each of these observations are called a *Long Run* in the CoRoT jargon. Since February 2007, the beginning of science observations, CoRoT has carried out 5 long runs. In each of these fields, the CoRoT consortium has identified numerous planetary candidates. Intensive multi-site and

⋆ Based on observations made with HARPS spectrograph on the 3.6-m ESO telescope and the EULER Swiss telescope at La Silla Observatory, Chile.

⋆⋆ The HARPS results presented in this paper (Appendix A) are available in electronic form at `http://www.aanda.org` and at the CDS via anonymous ftp to `cdsarc.u-strasbg.fr (130.79.128.5)` or via `http://cdsweb.u-strasbg.fr/cgi-bin/qcat?J/A+A/506/303`

Table 1. Main parameters of CoRoT-7 from Léger et al. (2009).

RA (2000)	06:43:49.0
Dec (2000)	–01:03:46.0
V-mag	11.67
$B-V$	0.86 ± 0.03
Spectral type	G9V
Age	1.2–2.3 Gyr
Distance	150 ± 20 pc

multi-instrument ground-based follow-up programs (Bouchy et al. 2009) have been organized for all of these candidates.

During the first long run in the direction of the anti-center of the galaxy (LRa01) from October 2007 to March 2008 a small transit signal of 0.3 mmag (0.03%) of 1.3 h duration with a period of 0.8535 days was identified in the CoRoT light curves. This detection immediately triggered a series of follow-up observations to clarify the origins of this shallow transit signal. This detection and the follow-up campaign is reported in Léger et al. (2009), with the exception of the high precision analysis radial velocity measurements that were carried out with the HARPS spectrograph and that are the subject of this paper. For convenience we list the main parameters of CoRoT-7 in Table 1.

In this paper we describe follow-up measurements of CoRoT-7 with the HARPS spectrograph that were made after the transit detection in the CoRoT light curve. The radial velocity investigation was complicated by the stellar activity of CoRoT-7. An analysis is presented that includes ground-based photometry that is needed to understand the origin and the temporal structure of the stellar activity. The data were processed in various manners to extract a robust quantitative estimate of the Doppler signature induced by orbiting bodies. From this work we present independent evidence establishing the planetary nature of CoRoT-7b transit detection. The mass of CoRoT-7b is measured within a 20% accuracy. From the radial velocity data we show the presence of another planet, CoRoT-7c . If one assumes that both planets are on coplanar orbits, the CoRoT-7c (the second planet) also belongs to the category of super-Earth planets.

2. Observations

2.1. The HARPS data

The first spectroscopic observations of CoRoT-7 were made in the Spring 2008 using SOPHIE on the 1.93 m telescope at OHP (Léger et al. 2009) and then HARPS on the 3.6 m telescope at La Silla. This was done as part of the regular systematic follow-up activities conducted on all CoRoT transit detections. These first measurements could exclude the presence of a stellar companion (grazing eclipse) but were insufficient for detecting the Doppler signature of the planet. Subsequently, further photometric and spectroscopic observations established with high probability that CoRoT-7b was indeed a transiting planet (Léger et al. 2009). This triggered a very extensive campaign of radial velocity measurements during the next season (2008–2009) when CoRoT-7b was visible again. Thanks to the combined effort from the HARPS exoplanet survey program 082.C-0120 (Mayor et al. 2003), program by Hatzes et al. 082.C-0308(A) and a granted DDT program by Bouchy et al. 282.C-5036(A), more than 70 h of observations have been gathered for this star.

A total of 106 measurements were obtained over 4 months, and on several occasions 3 well-spaced observations were made on the same night. The exposure times were between 30 and 60 min and were selected so as to reach a typical signal-to-noise ratio (S/N) of 50 per pixel at 5500 Å. All observations were carried out in single object mode, without the second fiber fed by the Thorium spectrum. The "extreme precision" (1 m s^{-1} or below) was not required since the corresponding radial velocity error for $S/N = 50$ spectra is about 2 m s^{-1}. Furthermore, the radial velocity measurements were affected by additional "noise" due to stellar activity. Errors on other spectral parameters like the bisector and on the full-width-half-maximum ($FWHM$) of the cross-correlation function (CCF) were fully dominated by photon noise as well. Systematic effects on the spectral shape from instrumental instability may be considered as negligible. Observations of many quiet FGK dwarfs with HARPS over several years show that the CCF parameters remain highly stable over the long term. As an example, $FWHM$ values have rms dispersions below 4 m s^{-1} for many stars. This demonstrates the high stability of HARPS in general, and of its instrumental profile in particular. Instrumental systematics in the CCF parameters can therefore be considered negligible in the case of CoRoT-7, particularly over the relatively short time span of the observations.

Besides accurate radial velocity measurements, HARPS can provide additional information on the spectral line shapes that are extracted from the CCF. (The CCF can be considered to represent the average shape of all spectral lines of the star.) Any changes in the CCF that are correlated with the radial velocity can be immediately attributed to pulsation effects or stellar spots both of which affect the shapes and thus the centroids of the spectral line. Thanks to the unique "built-in" stability of HARPS, changes in the detailed shape of the CCF may be used as an indicator of intrinsic stellar variability. Technically speaking, one uses two simple diagnostics to look for changes in the shape CCF: its width ($FWHM$) and its bisector span (hereafter bisector) computed according to Queloz et al. (2001). The HARPS wavelength coverage also includes the CaII H&K lines, so the activity S-index (Mount Wilson System) is computed as well. The spectroscopic S-index is sensitive to active regions on the stellar surface. The Ca II H& K flux that is converted to the Mount Wilson system according to Santos et al. (2000) and corrected for the photospheric flux is known as $\log(R'(HK))$ index. In summary, HARPS provides three ancillary measurements that can be used to monitor intrinsic variability of the star: the bisector span of the CCF, the $FWHM$ of the CCF, and the Ca II S-index.

Obvious signs of variability in the spectral line shape, $\log(R'(HK))$ activity index, and radial velocity are detected in CoRoT-7 (see Fig. 1). The radial velocity measurements have a 10 m s^{-1} rms scatter with 40 m s^{-1} peak-to-peak excursion, and they show clear multi-periodic variability structures. If the star's velocity were due to a planetary companion, then the shape of the stellar lines (CCF) should remain constant. On the other hand, radial velocity variations caused by stellar variability should correlate with changes in the spectral line shapes and/or Ca II. In the case of CoRoT-7, all parameters vary, which complicates the extraction of any planet signal from the intrinsic stellar variability. It is worth noting that the variation in the CCF width ($FWHM$) is rather smooth and shows a clear periodic pattern of about 25 days. Indeed, in the periodogram analysis of all the spectroscopic data (radial velocities, $FWHM$ of the CCF, Ca II H& K, and bisector span) a dominant peak is found at 23 days, the rotation period of the CoRoT-7 (Léger et al. 2009).

The $\log(R'(HK))$ activity index has a mean value of −4.612 with a 2% peak-to-peak variability. From the mean activity index value, the rotation of the star is estimated at 23.6 days

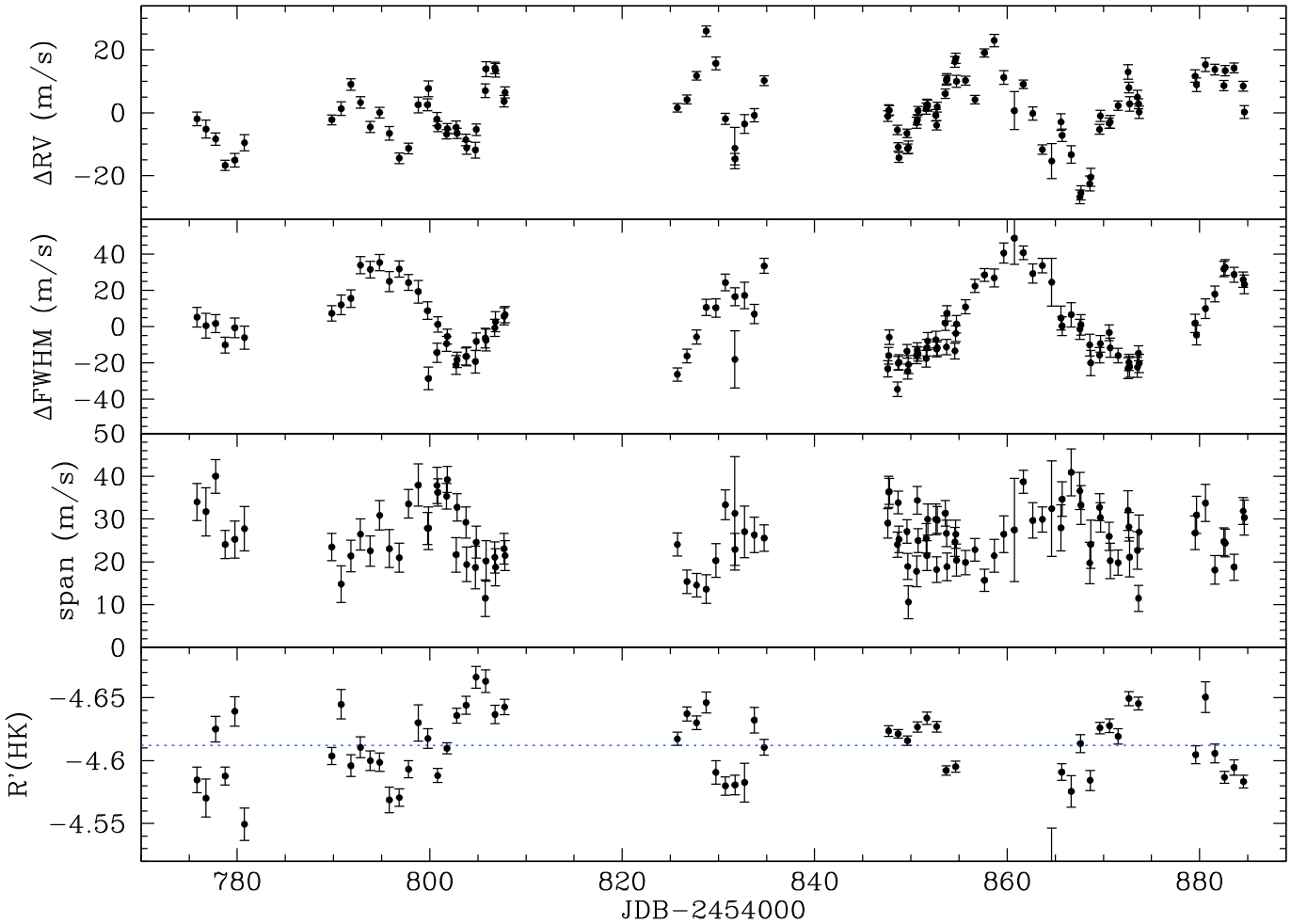

Fig. 1. A synthetic view of the radial velocity and spectroscopic information measured from HARPS data from November 2008 to February 2009. The dotted line in the bottom diagram indicates the average $R'(HK)$ index.

(Noyes et al. 1984), in close agreement with the 23 days value inferred from the Corot light curve. This close agreement may be fortuitous considering the uncertainties in the systematics of the Noyes et al. (1984) calibration.

Stellar magnetic activity in the form of starspots is well known by planet Doppler hunters to generate radial velocity "jitter" or scatter in their data. Saar et al. (1998) presents a model for estimating this scatter from the rotational velocity and spot filling factor of the star. Using the measured projected rotational velocity and photometric amplitude variations for CoRoT-7, a radial velocity rms scatter of 8 m s^{-1} is expected, which is comparable to the measured radial velocity scatter. Therefore, to detect the signature of the CoRoT-7b transiting planet, one should as well include stellar activity when analyzing the radial velocity measurements.

2.2. EULER photometry

During the course of the intensive HARPS observation campaign, it became obvious that to identify a clear radial velocity signature from CoRoT-7b we should obtain a better understanding of the impact of the stellar activity on our measurements. Ground-based photometric measurements that were simultaneous to the HARPS measurements were carried out at the Swiss Euler Telescope from the end of December 2008 to the beginning of February 2009. Since both telescope are located at La Silla, the difference in the weather conditions between sites was not a concern.

The Swiss Euler telescope photometry was carried out in a series of short exposures of about 20 min. In Fig. 2 one sees that both the color $(B - V)$ and the stellar magnitude vary. It is interesting to note that this variability pattern matches the extrapolation of the CoRoT light curve if assuming a rotation period of 23.64 days and a shift of 17 full rotation cycles to the time when spot effects were most visible in the CoRoT data. The relation between the $(B - V)$ index and the magnitude may be simply understood by cool starspots on the stellar surface. When an active region is facing the observer, both the average temperature and the luminosity of the star are decreased. As a result the magnitude increases ($\Delta V > 0$) and the star becomes redder $\Delta(B - V) > 0$.

Another important outcome of this simultaneous sequence is that, when the photometric signal is compared with the variation of the CCF width, a linear correlation between these two parameters is found (Fig. 2). The relation between the CCF width and the stellar flux is consistent with a rotating cool spot scenario as well. The cross-correlation function corresponds to the mean shape of lines in the stellar spectra. The change in the width of the CCF therefore reflects an average modification of the line widths. A cool spot acts as a shadow on the stellar disk and affects the rotational line profile. For a fast-rotating star one can see spectral distortions. When the spot is

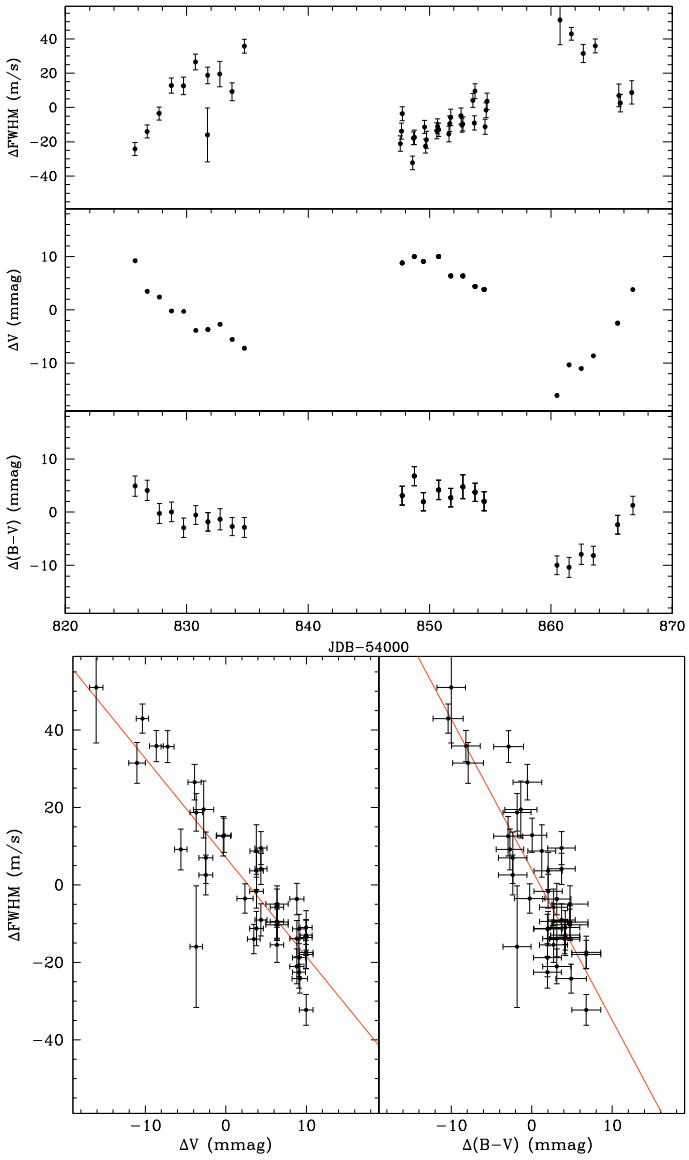

Fig. 2. Swiss Euler telescope photometric measurement obtained simultaneously to the HARPS measurements of the CCF width (*FWHM*). *Top*: time series of the photometric variations for CoRoT-7 computed from an average of short series of exposure totaling 20 min. Also shown are the contemporaneous HARPS *FWHM* measurements. *Bottom*: correlation between the CCF line width and the stellar color and magnitude. The best linear fit to the data is illustrated by a superimposed line.

at disk center, you have a bump at line center and the wings appear broader. In this case, the *FWHM* of the line is a maximum when the spot is at disk center. When at the limb, the distortion is in the wings, making the line appear thinner. In addition, the width of the CCF is known to vary with the stellar effective temperature. In Santos et al. (2002), this effect has been carefully measured and empirically calibrated on a large sample of stars. For main sequence stars, the smallest width is measured around $(B - V) = 0.87$. Stars with colors on either side of this minimum have line width broadening mechanisms that increase with a change in effective temperature. CoRoT-7b is slightly bluer than $(B - V) = 0.87$, therefore when the main spot region becomes visible, a decrease in both of the average luminosity and of the average temperature of the visible stellar photosphere is expected. Therefore when the star is dimmer, it is redder and the average line width decreases. Fitting a linear relation to the data one obtains: $\Delta(FWHM)\ \mathrm{km\,s^{-1}} \sim 2.55\Delta V$ and $\Delta(FWHM)\ \mathrm{km\,s^{-1}} \sim 3.89\Delta(B - V)$.

The interesting consequence of the linear relation between the *FWHM* of the CCF and the stellar luminosity variability is that we can get an estimate of the level of the stellar variability from the *FWHM* measurement without the need to carry out simultaneous photometric measurements. One also can look for other correlations between parameters to better identify and characterize the activity signal in our radial velocity data which is the topic of the next section.

3. Blind analysis of the data

In this section we analyze the time structure of the data keeping in mind a possible composite scenario including planets and starspots to describe our radial velocity observations. Starspots are well known to produce radial velocity variability, as well as spectral line variations. The analysis carried out in this section does not assume any specific geometric configuration causing these variations. It is, in that sense, a blind approach where we let the data speak for themselves.

Starspots are often grouped in "active regions". The typical lifetime of these regions depends on their size (Donahue et al. 1997). For our Sun, active region's lifetimes range from a few days to 60 days. Sometimes they are part of long-lived active complexes (or "active longitudes") that are constantly replenished by the formation of new active regions without phase disruption, while the amplitude may have drastically changed with a near-quiescent phase between more active periods (Castenmiller et al. 1986). It is therefore important to keep in mind that the periodicity and the phase coherency of a signal does not preclude it from originating from stellar activity. However one would expect such a stellar activity "signal" made up of rotating active regions to be simultaneously detected in the radial velocity, in the spectral line shape variations, and in the photometry.

3.1. Correlation between parameters

The first obvious correlation to look for when activity may be at play is the bisector span (V_{span}) versus the radial velocity, V_{r}, (Fig. 3). The bisector span exhibits a 6.75 $\mathrm{m\,s^{-1}}$ rms and a weak correlation with radial velocity variation ($V_{\mathrm{span}} \sim -0.19(\pm 0.06)\Delta V_{\mathrm{r}}$). The anti-correlation between these two parameters corresponding to the negative sign of the slope is expected for rotating cool starspots, but the slope is shallower compared with similar measurements on other active stars like HD 166433 (−0.88) or HD 189733 (−0.61) (Queloz et al. 2001; Boisse et al. 2009). In Fig. 3 there is a significant scatter ($6.5\ \mathrm{m\,s^{-1}}$) that is not correlated with the radial velocity. A similar residual scatter above the measurement errors has been found in the active star HD 219828 (Melo et al. 2007), which was also observed with HARPS. The weakness of the coupling between the bisector and the radial velocity variation for slow-rotating stars is a known phenomena traditionally pictured as a "magnification" effect with increasing $v \sin i$ (Saar et al. 1998). For slowly rotating stars, this makes the bisector less useful than anticipated for tracing the stellar activity related radial velocity variation pattern.

To explore other relations we computed the correlation between various parameters using a slightly different version of the discrete correlation function of Edelson & Krolik (1988, see also White & Peterson 1994) for unevenly spaced data. The

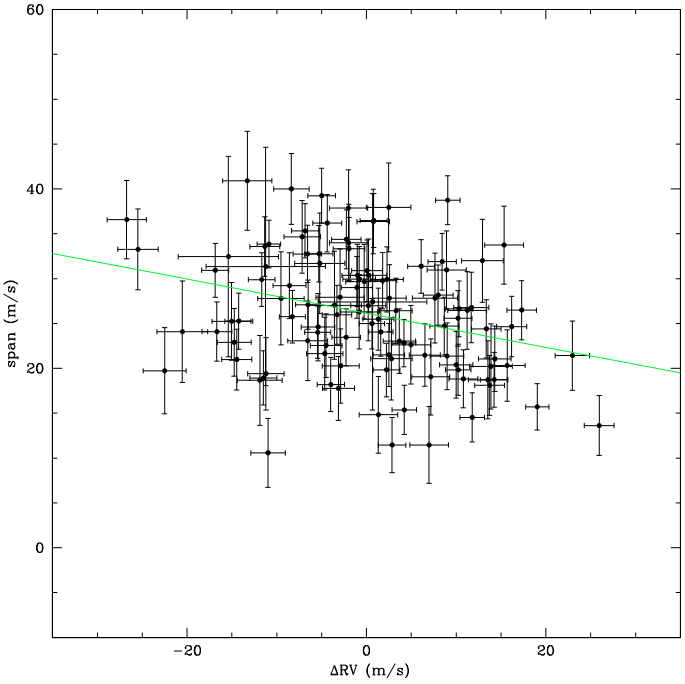

Fig. 3. Diagram of the correlation between the bisector span of the CCF profile and the radial velocity. By fitting a linear relation one finds a significant negative slope of -0.19 ± 0.06 (solid line).

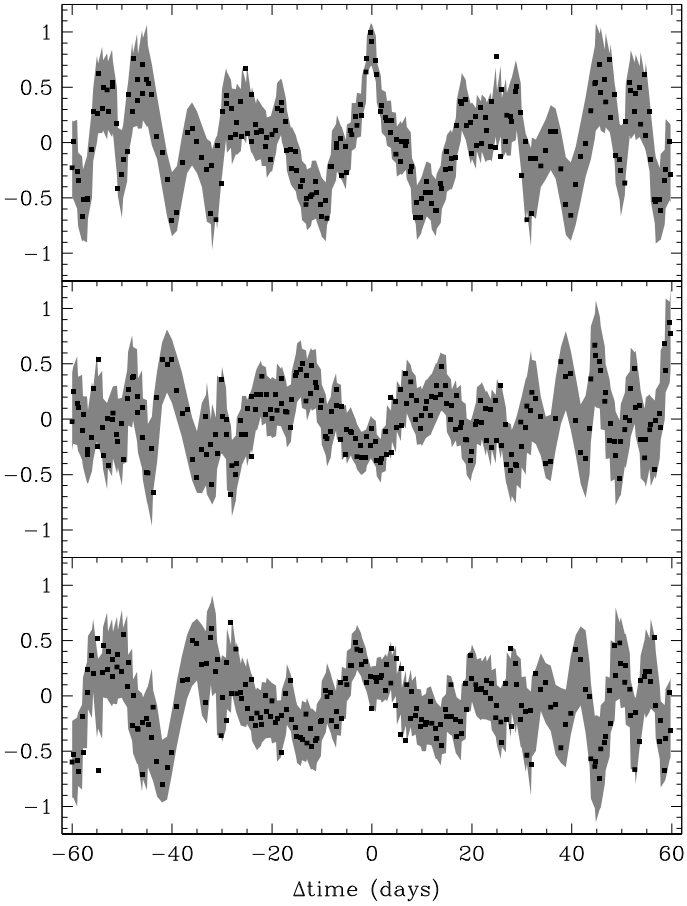

Fig. 4. Autocorrelation between two parameters with a time delay. *Top*: autocorrelation of the radial velocity measurements. *Middle*: correlation between radial velocity and *FWHM* of the CCF. *Bottom*: correlation of the line bisector and the radial velocity measurements. The hatched area indicates the $1 \pm \sigma$ uncertainty smoothed with a 3-day box. The errors are computed according to $1.5/\sqrt{(n_i)}$, where n_i is the number of points found in each lag.

(auto-)correlation of the radial velocity measurements with itself in Fig. 4 (top) reveals a central peak width of about 5 days and a pattern with a minimum (or anti-correlation) at 11 days, and then a second peak around 25 days. After this point the correlation function becomes more complex, but one can still see a similar structure (a second cycle) going first to a minimum and another about 25 days later. This structure, while noisier, can still be distinguished in a third cycle. This pattern agrees overall with a 23-day period rotating star with an active region slowly varying in time.

We looked for possible correlations between the radial velocity and CCF width and shape (bisector span) measurements and considering a time lag between them (Fig. 4). In all cases one again sees a 23 day periodic pattern suggesting that the rotation period is the strongest component in the signal. Interestingly, the maximum correlation between the radial velocity and the CCF width does not occur at the same time, but when one applies a time lag of about 15 or 7 days (depending on the sign). This observed lag means that the *FWHM* variability pattern is seen about 15 days (±5d) later in the radial velocities signal, corresponding to about 3/4 of the rotation period (or equivalently −1/4 the rotation period). We tested this correlation as well by fitting a synthetic multi-component sine-curve to the *FWHM* variations. To correct the phase shift, we added 5.8 days (1/4 of the rotation period) to each *FWHM* fitted value (corresponding each to real measurements). This way the 3/4 rotation phase delay is corrected by moving the *FWHM* data one full rotation phase ahead. With this correction, the lag-corrected data set shows a linear correlation between *FWHM* and the radial velocity with a linear regression of −0.62, while no significant correlation is measured without adding this time delay.

The correlation signal between the bisector span and the radial velocity exhibits a clear anti-correlation after 15 day. It suggests as well a small offset of a few days between the two variation patterns. It is difficult to understand the significance of these time delays without a complete modeling of the cross-correlation profile that goes beyond the goal of this paper. Our general understanding is that there are time-structured variations between these two parameters that are expected in a spotted atmosphere like CoRoT-7.

In conclusion, the variations in all these parameters are dominated by the rotation pattern of stellar surface structure. These may be understood to the first order as the effect of cool spotted regions on the rotating stellar surface of CoRoT-7. When the spot area is visible, both the luminosity and the *FWHM* of the CCF are a minimum as well. When the spot area is behind the star, both the luminosity and the *FWHM* are at maximum. When the spot is on the approaching limb (hiding part of the blue side) the radial velocity is maximum and when it is on the receding limb (hiding part of the red side) the radial velocity is at a minimum, see figure in Queloz (1999).

The geometry of the activity resulting from our analysis agrees with a more sophisticated model of CoRoT-7 established from the measured light curve. This modeling also suggests that a dominant spot region with a lifetime of at least 60 days and random individuals spots with shorter lifetimes than the rotation period (Lanza et al., in prep.).

3.2. Pre-whitening analysis of the radial velocity data

As a simple, first approach we investigated the structure of the radial velocity signal using a *pre-whitening procedure* (or CLEAN method) based on a Fourier transform (FT) frequency analysis. This technique is often employed in the analysis of multi-periodic stellar oscillations. It makes the assumption that signals are coherent, long-lived, and sine-shaped. (Note that a non-sinusoidal signal can be represented as a sum of Fourier components.) In this process a Fourier analysis is used to find the highest peak in the power spectrum. A sine fit with this frequency is subtracted from the data and another Fourier analysis performed on the residuals. This yields the next dominant frequency for removal. The subtraction of subsequent dominant components is continued until the level of the noise is obtained. Because of the data sampling, each real frequency is accompanied by alias peaks, so we cannot be 100% sure which peak is the true one. Noise and sampling may result in a true peak having a lower amplitude than an alias or noise peak. Throughout the procedure we simply assumed that the highest peak in the residual FT was the true frequency.

The pre-whitening procedure was performed on the radial velocity data set. Given the complexity of the radial velocity signal, examining a time series with a longer time base increases the chances of detecting weak signals in the presence of stronger ones, particularly if these are long-lived and coherent. The procedure used the program Period04 by Lenz & Breger (2004). After finding all significant frequencies, a least squares solution using all frequency components was performed. Kuschnig et al. (1997) established that peaks that are more than 4 times the Fourier noise level have a false alarm probability of less than 0.01. The noise level of the HARPS radial velocity data, measured at high frequencies, is about 0.4 m s^{-1}. Thus peaks with amplitudes less than about 1.6 m s^{-1} were considered to be noise.

Because the Nyquist frequency is about 0.5 c d^{-1}, one normally should not chose peaks beyond one cycle per day when only a few measurements are carried out each night. In addition, frequencies over one cycle per day are usually the $1 + \nu$ alias of a shorter "true" frequency signal, so for most of the pre-whitening procedure, only peaks in the FT signal below 1 c d^{-1} were considered as the true ones. The one notable exception was the 0.8535 d transit period (1.1716 c d^{-1}) detected by CoRoT. During the pre-whitening procedure we actually found a peak at 0.168 c d^{-1} and its alias at 1.1716 c d^{-1}, which coincidentally had a higher amplitude. Since the latter is close to the transit frequency, it was selected.

Table 2 shows the results of the pre-whitening procedure. Figure 5 displays the fit of the radial velocity data using the frequencies listed in Table 2. For clarity the radial velocities are shown in subsections of time and with differing scales where appropriate. The rapid variations stem from to the 0.85 day period. Although radial velocity data is undersampled for this period, on nights when repeated measurements were made, the radial velocity follows the expected short period variations quite well. The rms of the data about the final fit is 1.81 m s^{-1}, consistent with the the mean error of 1.84 m/s for the HARPS radial velocity data.

The most dominant frequency was found at 23.15 days and corresponds, as expected, to the rotation period. Then two frequencies of equal amplitude were found at 9 days and 10 days. At the fourth rank, an isolated signal at 3.69 days with an amplitude of 5 m s^{-1} was found, and then at the fifth position, a periodic signal with an amplitude of 4 m s^{-1}, at the same period as the CoRoT-7b transits. After correcting the first five strongest signals, a 28 day periodicity is measured above 5 m s^{-1} amplitude. All remaining signals are equal to or below 3 m s^{-1} amplitudes.

Table 2. Frequencies and amplitudes of the radial velocity measurements found by the pre-whitening procedure.

Frequency (c d^{-1})	Period d	Amplitude (m s^{-1})	Phase
0.0432	23.15	7.50	0.87
0.1108	9.03	6.20	0.83
0.0944	10.6	5.69	0.05
0.2706	3.69	5.02	0.22
1.1702	0.854	4.36	0.16
0.0363	27.6	5.68	0.38
0.1814	5.5	3.10	0.61
0.0716	14.00	3.26	0.64
0.2516	3.975	1.78	0.38
0.1373	7.28	1.85	0.88
0.1649	6.06	1.97	0.53
0.0228	43.8	2.14	0.75
$\sigma = 1.81$ m s^{-1}			

Many of the frequencies in Table 2 may be associated with the stellar activity signal. For instance $P = 10.6$ d, $P = 7.3$ d, and $P = 5.5$ d are near the first three harmonics of the rotation period. Some frequencies are obviously harmonically coupled like series $P = 27.6$ d, $P = 14$ d and $P = 7.3$ d. In addition, amplitude variations of a single period may produce an observed combination of closely-spaced, but false frequencies. (Conversely, an observed amplitude variation in a single frequency may come from merely to two closely-spaced frequency observed with poor sampling.) This effect is usually called the "two-frequency beating mode" and it is well studied for δ-Scuti stars (see references in Breger et al. 2006). The resulting beat frequency is $\nu_2 - \nu_1$. If one considers the two close periods 10.6 days and 9.0 days they may be related to amplitude modulations of a single period of 61 days. Interestingly, two months is the observed duration of lifetime of the starspot group (see next chapter). One can therefore not exclude a radial velocity envelope variation of about 60 days being at the origin of the detection of these two frequencies.

For these frequencies, additional arguments pointing towards stellar activity origins is provided by the detection of similar frequencies in periodogram analysis of the CoRoT light curve (see next chapter, Table 3), as well of strong anti-correlations between the radial velocity and the bisector span or breaks in the phase of the signal during some periods. Some of these frequencies may be found as well in the FT frequency analysis of the *FWHM* of the cross-correlation function. Furthermore a Fourier analysis of the *FWHM* measurements reveals a peak at ~30 days. No detail analysis of all these relations is made in this paper. Our sole purpose is to identify their stellar activity origins.

Out of all modes listed in Table 2 with an amplitude greater than 3 m s^{-1}, only two of them cannot be connected to a stellar activity signal: $P = 3.69$ days and $P = 0.854$ days (the CoRoT-7b transit period). Keplerian motion from orbiting planets may be the origin of these two periods. To develop this possible scenario further, the activity signal must be better identified and filtered out from the data.

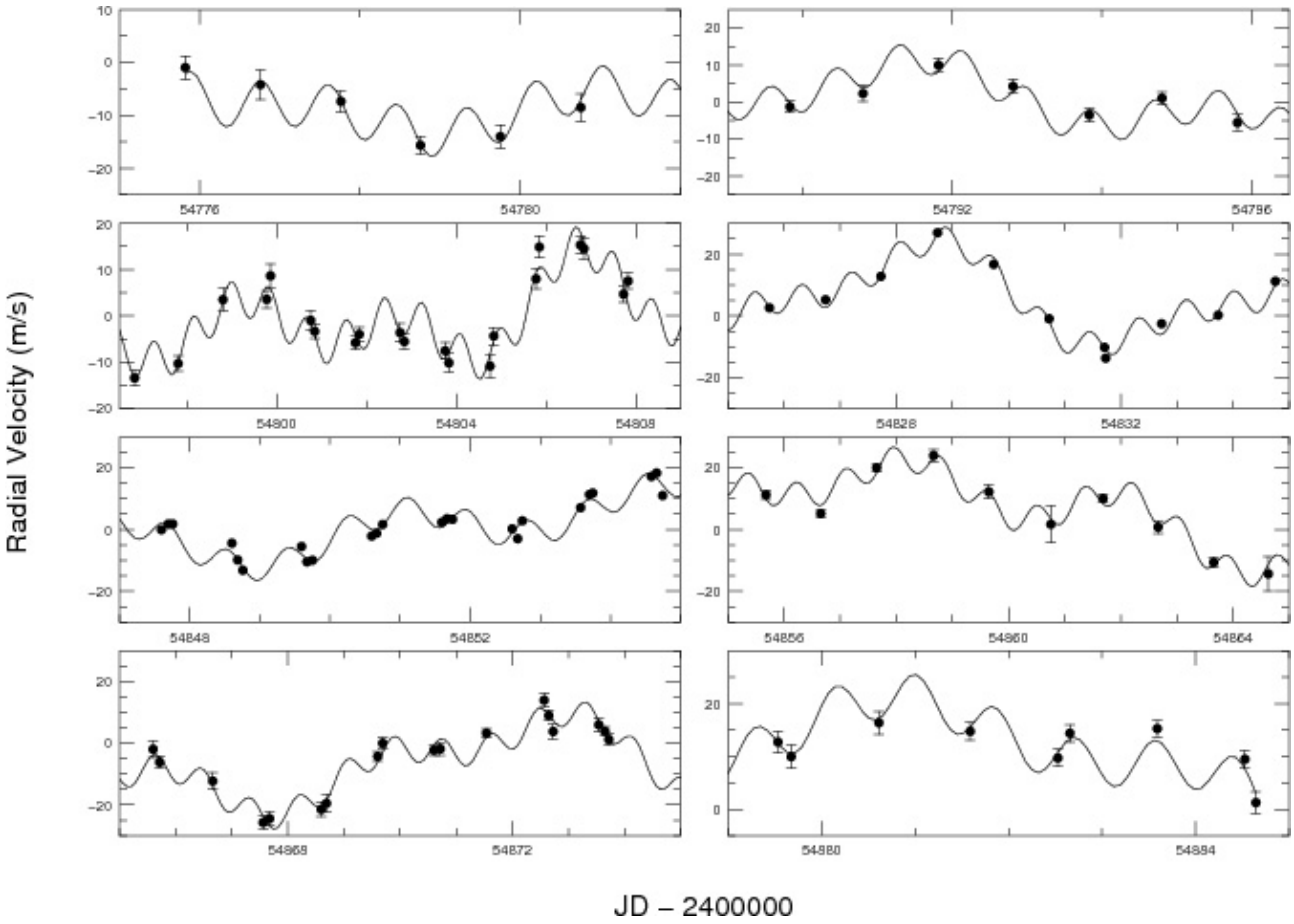

Fig. 5. Display of subsets of radial velocity measurements of CoRoT superimposed with the global solution obtained from the pre-whitening procedure using the parameters listed in Table 2.

4. Filtering out the activity

The dominant effect causing the radial velocity variation is the stellar rotation. This activity-related variability may be represented as a series of harmonics of the rotation period bounded by a coherence envelop that depends on both the strength (or number) and lifetimes of starspots on CoRoT-7. With this model in mind, we decided to fit the activity signal by fitting the amplitude of the first rotation harmonics ($P_{\rm rot}$, $P_{\rm rot}/2$, $P_{\rm rot}/3$,...) over a limited time range (length of the time window) moving through the whole series of data. Physically, one can interpret a harmonic, such as $P_{\rm rot}/2$, as arising from two equally-spaced spot groups (and $P_{\rm rot}/3$ from three, etc.). Alternatively, one can consider the harmonic terms as additional Fourier components needed to fit a radial velocity curve that departs from pure sine wave.

For each of the observed data $d(i)$, we obtain a series of fits $\{f_j(t)\}$, (where j indicates the corresponding used time window) obtained by the scan of the corresponding window through the full data range. Data at the edge have less fitted values since the scan is limited by the data boundary. With all series of fits, one can compute the mean fitted $F(t)$ value for each data point and its residual. These mean fitted values of $F(t)$ are our measurement of the activity signal estimated from the mean of harmonic decompositions from the data over a limited length of the time window. Our activity model is made of three parameters: the rotation period $P_{\rm rot}$, the length of the time window (coherence time), and the number of harmonics. As a result, in addition to the amplitude of the activity, the model also provides the variation in the phase and amplitude of each harmonics with time. It does not assume any specific spot geometry distribution and does not aim to provide a "picture" of the stellar photosphere. In that sense we may consider our approach as independent of any model describing the geometric distribution of active regions on CoRoT-7b.

We first applied this modeling to the CoRoT light curve of CoRoT-7 to check the capability of the model to adjust the variability of the light curve and to optimize the coherence time parameter. With a set of first-guess parameters we explored the number of harmonics needed, and it was obvious that the signal could be perfectly reproduced with the three first harmonics alone ($P_{\rm rot}$, $P_{\rm rot}/2$, $P_{\rm rot}/3$). This is in full agreement with the Fourier analysis of the Corot light curve where only the first three rotation harmonics are detected. The amplitude of each harmonics decreases with its mode numbering (see Fig. 7 and Table 3 for the corresponding list of frequencies extracted by CLEAN algorithm analysis).

The smallest scatter between the series of solutions is obtained with a rotation period of $P = 24$ day and with a one day uncertainty. Rotation periods below 23 d or above 25 d increase the scatter. For example the scatter is increased by 50% with a 22-day rotation period. That a 10% change in the rotation period has such a drastic effect on the quality of the fit is an additional element demonstrating the limited free range available for this important parameter. The search for the best value of the coherence time was done keeping in mind that the starspot lifetime is

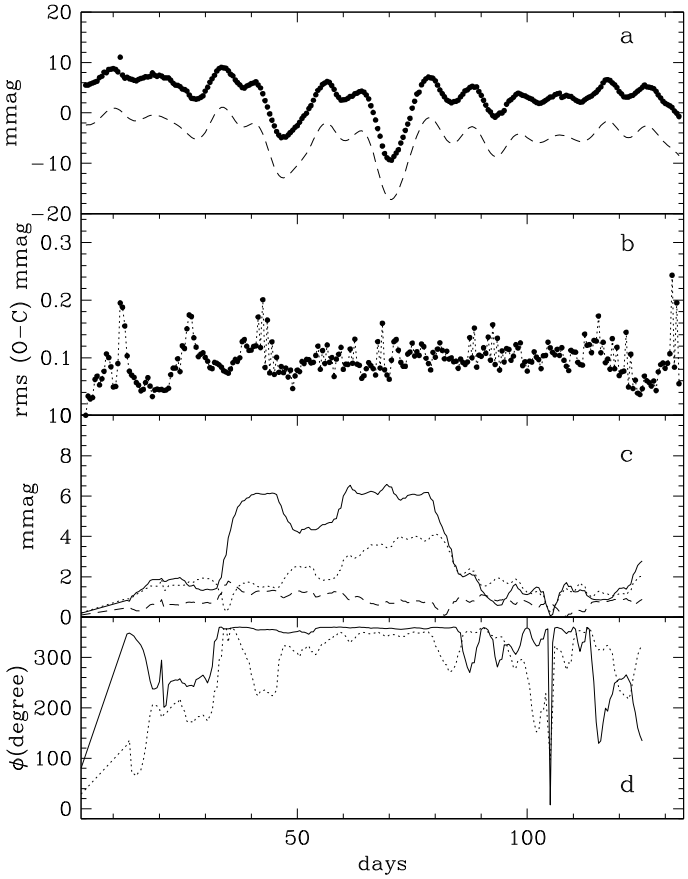

Fig. 6. Harmonic fit of the Corot light curve. Only the first three harmonics have been considered (P_{rot}, $P_{rot}/2$, $P_{rot}/3$); **a)** solid line: Corot light curve smoothed by a 20 min width box-filter, hatched line: fitted signal. Both curves have been moved by ±4 mmag for clarity; **b)** rms value of each series of fitted solution for each point of the fitted signal displayed above; **c)** amplitude of the harmonics with solid line: P_{rot}, dotted line: $P_{rot}/2$, hatched line: $P_{rot}/3$; **d)** phase of the two most dominant harmonics: solid line: P_{rot}, dotted line: $P_{rot}/2$. The last phase and amplitude displayed is when the end of the time window length range (coherence time) reaches the end of the data sequence.

Table 3. Frequencies and amplitudes of the CoRoT light curve when the CoRoT-7b transit is removed.

Frequency (c d^{-1})	Period d	Amplitude (mmag)
0.0463	21.6	2.9
0.0367	27.2	2.3
0.0925	10.8	1.2
0.0830	12.0	1.4
0.0554	18.0	1.0
0.0711	14.1	0.9
0.1281	7.8	0.5
0.0986	10.1	0.6
0.1059	9.4	0.5
0.0768	13.0	0.5

Results listed in this table are only in the period range listed in Fig. 7 and for peaks with amplitude larger than the correspond value for a false alarm probability (FAP) of 5σ.

close to the rotation period. We found that below a 17-day coherence time there is little improvement in the fit residuals, but above 19 days there is a significant degradation of the signal, so we settled for using 18 d. The result of our harmonic modeling

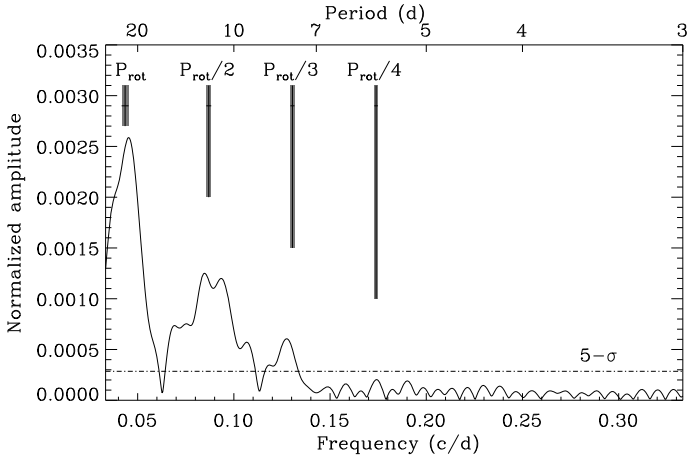

Fig. 7. Fourier transform analysis of the CoRoT light curve for periods between 3 and 30 days. The frequency harmonics of the rotation period (23.5 ± 0.5 day) are indicated. Hatched line indicates the 5σ detection false alarm probability computed from the statistic of the average level measured between 0.2 and 0.5 d. The identification of relevant frequencies are listed in Table 3.

of the light curve is displayed in Fig. 6. The signal analysis of CoRoT-7 light curve suggests that its stellar surface is dominated by a starspot group that shows little longitude change during two months and then vanishes. Outside this phase of activity, series of weak and short-lived spots are detected at random locations. The abrupt phase variations, when the amplitude of the harmonic drops below 0.5 mmag, must be considered as noise.

This picture derived from the harmonic modeling of the light curve is consistent with the blind analysis of the radial velocity data both as a general picture of stellar activity on the surface of CoRoT-7, as quantitative estimates of the rotation period and timescale of starspots. We then applied the same harmonic fitting algorithm on the radial velocity data with the assumption that the time structure of the radial velocity is triggered by the rotation cycle in a similar way than the light curve. We do not have a dense and continuous data set as in the CoRoT photometry. The data taken in the 2008–2009 season are made of five continuous sets of measurements. Fortunately the longest gap between them is 18 days. Relaxing the coherence time to 20 days allowed us to run our harmonic as a continuous and tight sequence and avoid artificial offsets between the different runs.

The harmonic adjustment with the resulting radial velocity variation residuals is displayed in Fig. 8. Technically speaking, the harmonic filtering removes all time components related to the rotation period and its harmonics. The use of 20-days time window length allows the fit to absorb slow amplitude variations and thus acts like a high-pass filter. In Fig. 8 we see that the major variability components are indeed modeled well by harmonics. This is expected, since we know from the previous chapter that the strongest variability frequencies are related to stellar activity.

The harmonic fitting procedure is not as efficient as the pre-whitening algorithm for extracting and removing all periodic signals present in the data. In addition with a coherence time of 20 days all possible longer periodic signals are destroyed. In spite of these limitations, the harmonic decomposition is robust against any signal not being harmonically coupled to the rotation period. It makes no assumption on the temporal structure of other periodic signal that remains uncorrected by the process as long as they are not coupled to the rotation period. It also uses fewer free parameters than the pre-whitening algorithm. In Fig. 8, in the residuals O–C of the harmonic fit, a variability

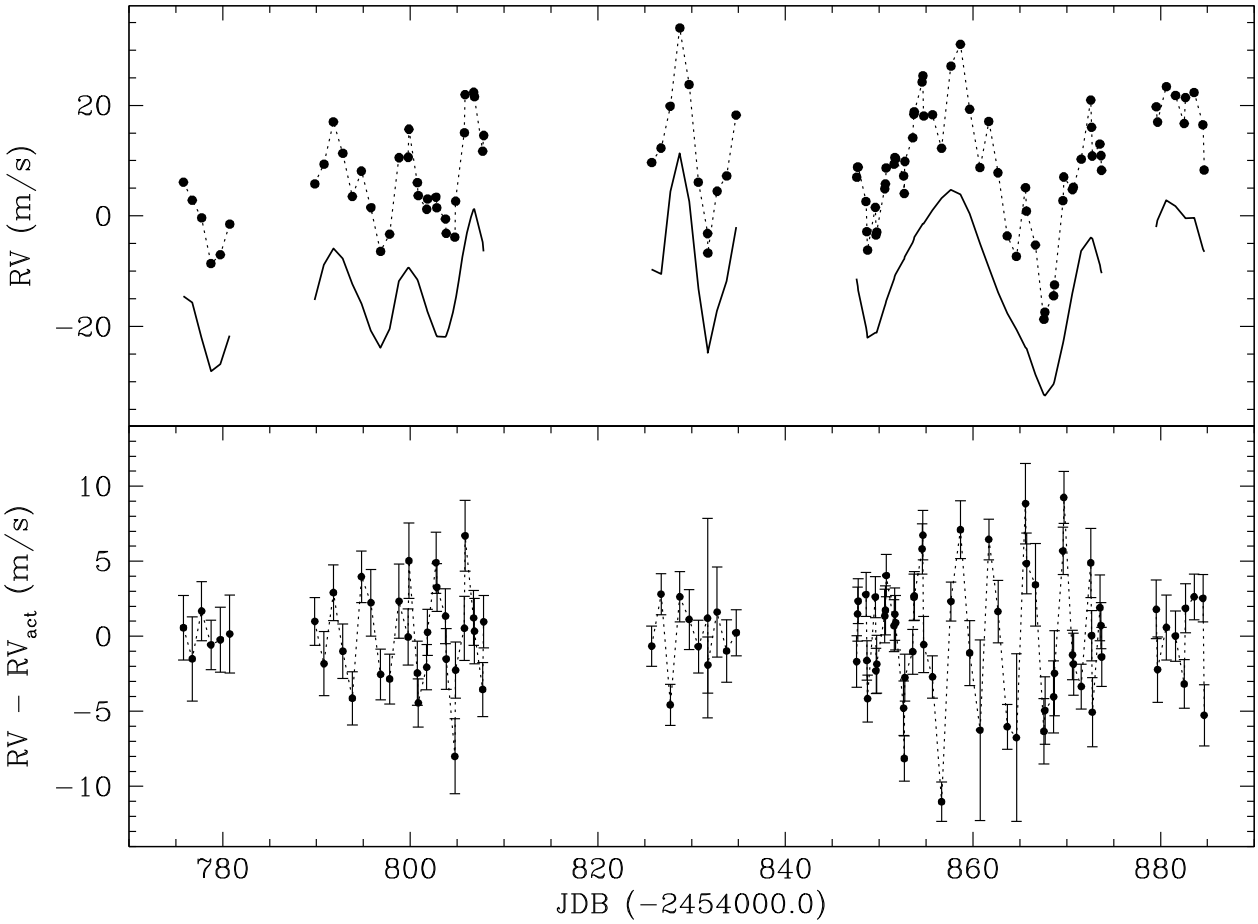

Fig. 8. *Top*: the radial velocity measurements (filled dots) with its fitted harmonics decomposition (solid line) using the first three harmonics of the rotational period. Similar to Fig. 6, both data sets have been shifted for clarity (by ±10 m s^{-1}). A time window of 20 day is used to fit the time series of data (see text for details); *bottom*: radial velocity data corrected from the stellar activity $V_{\rm rad} - V_{\rm act}$.

greater than the expected errors is visible, and a 4-day periodic signal may even be detected by eye.

5. Searching for planetary signature

It is obvious from the previous section that the dominant periodic signal in the radial velocity data comes from the activity effects related to rotating spots. From the pre-whitening results, at least two periods with amplitude between 4 and 5 m s^{-1} are obviously not related either to the stellar rotation or to the slow variation from spot evolution: $P = 0.854$ days corresponding to the CoRoT-7b transit detection and $P = 3.69$ days.

To conclude whether Keplerian motion from orbiting planets is the origin of this radial velocity variations, all activity components from the signal must be identified and removed. We looked at this question from two different perspectives to see if they produced consistent results. First, we used the pre-whitening results in combination with the transit ephemerides to detect the orbital signature of CoRoT-7b. Second, we looked for a signal in the radial velocity data filtered out by the rotation harmonic algorithm.

5.1. Detecting CoRoT-7b

The transit detection by CoRoT brings a severe constraint on the ephemerides of the orbiting planet. This is a strong element with little margin. For Keplerian motion, consistent orbital parameters should be found by using either the photometric or radial velocity measurements. To compare with the CoRoT-7b solution we removed from the radial velocity data all frequency components detected by the pre-whitening except that associated with the 0.85 d transit period. At this stage we do not address the origin of all these other signals. We only want to remove them to isolate the short-period one. An orbital solution was performed on the corrected radial velocity data using the CoRoT-7b, $T_{\rm t}$ transit time of 2 454 446.7311 for T_0. All other orbital parameters were allowed to vary, although the transit period was used as an initial guess. This result is displayed in Fig. 9 and listed in Table 4.

The orbital solution performed on the residual radial velocities (after removing all other sine components) found a slightly shorter period ($P = 0.85353 \pm 0.00002$) and smaller amplitude than was found in the the multi-component sine fitting using Period04. There is a slight eccentricity but the orbit is circular to within the error. Furthermore, slight changes in the shape of the radial velocity curve can be introduced by the filtering process, so this eccentricity may in fact be an artifact. The detection of this radial velocity signal with the constraint of the time of transit from CoRoT provides solid evidence that both the radial velocity variation and transit signal originates from the same periodic phenomena.

After obtaining an initial orbital solution, we then allowed T_0 to vary, but by fixing the period to the CoRoT transit period and the eccentricity to zero. This resulted in a $T_0 = 2\,454\,446.73196 \pm 0.00885$, which is consistent to the CoRoT transit ephemerides to within the errors.

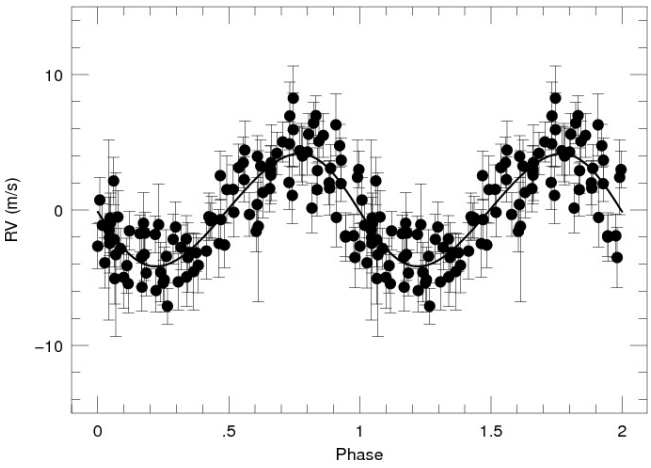

Fig. 9. Orbital solution for the 0.85-d period using the residuals from the radial velocity data after removing the contribution of all other frequencies detected by the pre-whitening procedure.

The pre-whitening process may affect the radial velocity amplitude we measure for CoRoT-7b. To investigate possible amplitude variations introduced by the filtering process, we performed another pre-whitening procedure, but this time we first fitted and then removed the 0.85 d component to the raw data. The pre-whitening procedure was then performed on the highest peak (the rotational frequency) and continued on the next highest peak in the residuals. With the addition of each new frequency, a simultaneous fit to the data was performed, and the amplitude of the 0.85-d period noted. The amplitude of the 0.85-day period varied between a maximum value of 5.8 m s^{-1} and a minimum value of 4 m s^{-1}. An uncertainty of about 1 m s^{-1} in the fitted radial velocity amplitude of the 0.85-d period can thus easily result from the filtering process.

We also tested how well the pre-whitening procedure could recover input signals of known amplitudes. For this simulation a simulated data set was calculated using all the frequencies in Table 2 except the one associated with the 0.85 d period. For the 0.85 d component, signals of different amplitudes were inserted into this fake data. This was then sampled in the same manner as the real data, and random noise at a level of 2 m s^{-1} was added. The noise characteristics in the data can affect the final radial velocity amplitude either in the fitted amplitude, or in our choice of frequency for removal. To account for this, 10 data sets for each input 0.85-d amplitude were produced using a different random number generator for the noise. As a result one found that the pre-whitening filtering artificially increased the amplitude of the 0.85 day signal. The "true amplitude" is about 80% of the measured value; therefore, the orbital solution gives an amplitude of 4.16 m s^{-1}, which corresponds to a 3.33 m s^{-1} "true" amplitude.

The orbital elements for the 3.7-day period (CoRoT-7c) are also listed in Table 4. Although the formal error on the amplitude is 0.3 m s^{-1}, the variations in the amplitude introduced by the filtering process can be as high as 1 m s^{-1}. This should be taken as a more realistic error. Again, the filtering process may overestimate the radial velocity amplitude so that the true amplitude is 80% less, which is the case for CoRoT-7b.

5.2. Detecting planetary signals in the data filtered for activity

In this section we look for periodic signals in the radial velocity measurements filtered from the rotational harmonics. To account for possible additional systematics arising from the filtering process, a 1.5 m s^{-1} error was quadratically added to our data. This additional noise corresponds to the measured scatter in the series of fit $\{f_j(t)\}$. We consider it as a typical estimate of the uncertainty on the activity component removed to the radial velocity data. In Fig. 10 a Lomb Scargle periodogram analysis of the harmonically filtered data shows a strong period at 3.7 days ($\nu = 0.271\,\mathrm{d}^{-1}$) with its series of aliases at ν+1, 1/(ν+1),... When an orbital solution is adjusted to these data with all free parameters, one finds a solution with $K = 3.4 \pm 0.4$ at $P = 3.6887 \pm .0089$ and $e = 0.17 \pm 0.13$. This period was identified as well by the pre-whitening algorithm.

Similar to the pre-whitening approach, we then removed the 3.7-day orbit from the data using the fitted orbital solution and then looked for a remaining signal in the residuals of the power spectrum decomposition. In Fig. 10 one sees that the 3.7 day peak with all its aliases are supressed and a significant and isolated peak is detected at $P = 0.853$ days ($\nu = 1.172\,\mathrm{d}^{-1}$) at the CoRoT-7b period (see zoom of the power spectrum decomposition in Fig. 10) with its usual series of aliases.

Fitting a circular orbital solution to the radial velocity residuals after removing the $P = 3.7$ days signal results in $P = 0.8516 \pm 0.00074$ days, $K = 2 \pm 0.4$ m s^{-1}, and $T_0 = 54\,447.463 \pm 0.34$, corresponding to time of transit $T_{\rm tr} = 54\,446.81 \pm 0.34$ in agreement with the CoRoT ephemerides. We looked for other possible signals in the residuals of this solution. In the power spectrum, of the residual no signal above a 10^{-4} (about 4–σ) false alarm probability was found. The radial velocity solution establishes the detection of the radial velocity signal of CoRoT-7b; however, a more precise constraint on the amplitude of the radial velocity signal (and the planet mass) may be reached when the CoRoT-7b period measured from the transit is assumed and kept constant in the orbit fitting.

In this analysis, CoRoT-7b is independently detected with the only assumption that the orbit is circular. Another small planet is detected at $P = 3.7$ days. To obtain a coherent solution, we simultaneously fitted a two-planet model to the data filtered from activity. To improve the quality of the adjustment we used the CoRoT-7b well-determined transit period ($P = 0.8536$ d). We did not use the CoRoT-7b time of transit $T_{\rm tr}$ as a fixed value since we suspected its accuracy to be degraded after more than 400 orbital cycles. Leaving this parameter free is also meant to assess the level of confidence in our solution. The solution is displayed in Fig. 11 and the results listed in Table 4.

The transit ephemerides measured by CoRoT compared to the radial velocity solution is off by only 1%. It is a very impressive match, considering that there is a one year gap between the CoRoT-7b transit measurements and the radial velocity data. Taking into account that more than 400 cycles have occurred in the meantime, this error would correspond to an uncertainty of less than 2 s (3×10^{-5} d) on the CoRoT-7b transit period. Formally we are statistically 2-sigma away if one considers the error quoted by Léger et al. (2009). However, we believe that this value may be slightly underestimated. Another way to express our slight difference is to compare it with the transit-folding process. A 10 s error on the period would correspond to 2% error on the phase folding between the first and the last transit observed by CoRoT. The accuracy of the CoRoT ephemerides is consistent with the orbital solution obtained in the pre-whitening processing that considered the CoRoT-7b time of transit as a fixed value.

The fitted amplitude of the CoRoT-7b radial velocity curve derived from the pre-whitening process differs from the one derived from the power spectra decomposition. To assess a possible effect of both the filtering and the fitting procedure, we

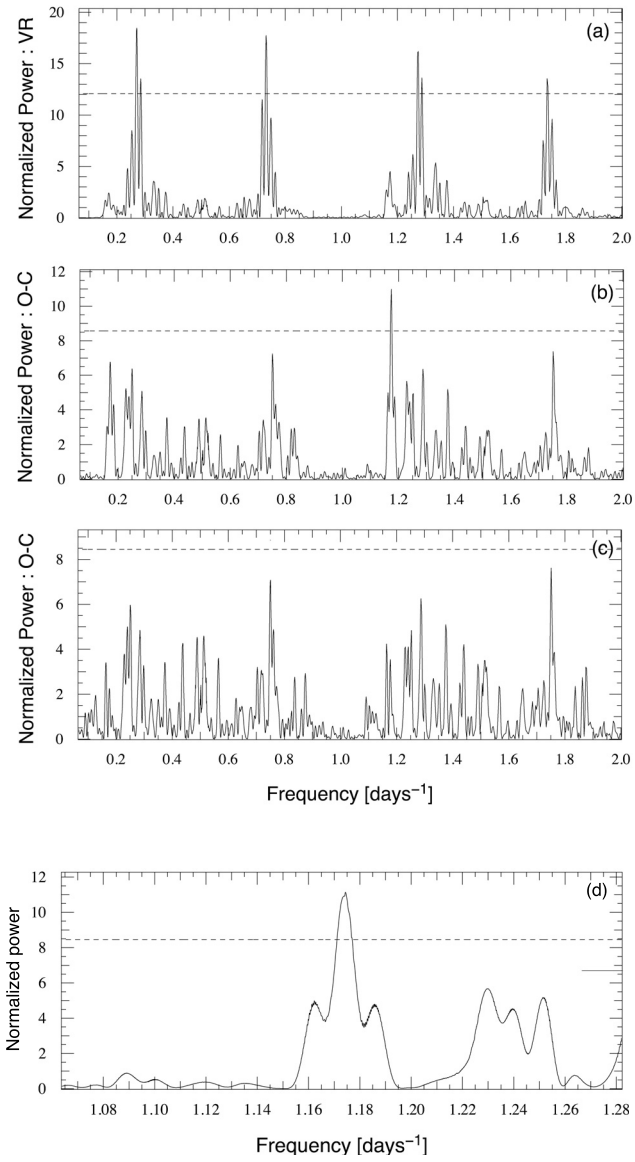

Fig. 10. Lomb Scargle periodogram analysis of the radial velocity data. The hatched line indicates the 10^{-4} false alarm probability. **a)** Periodogram of the radial velocity measurements filtered out from activity. The peak at $\nu = 0.27\,\mathrm{d}^{-1}$ corresponding to the 3.7 d period (CoRoT-7c) is clearly visible with its aliases. **b)** Periodogram of the radial velocity measurements filtered out from activity with the 3.7 d orbital solution removed. The period of the CoRoT-7b transit at $\nu = 1.172$ is clearly visible and its $\nu - 1$ alias peak not significant. **c)** Periodogram of the radial velocity residual after subtracting CoRoT-7b and CoRoT-7c orbital solutions. All peaks are below the noise floor. **d)** Zoom of the figure b around the $P = 0.85$ d region, showing the clear detection of the 0.853 d period of CoRoT-7b.

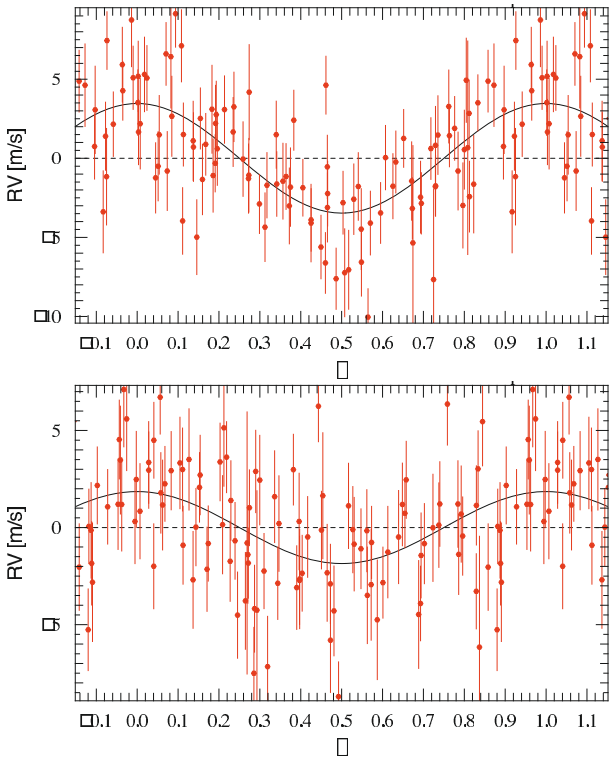

Fig. 11. Phase-folded solution of the two planet model computed from the radial velocity data corrected from the activity by harmonics decomposition: (*top*) CoRoT-7c , (*bottom*) CoRoT-7b. Fitted parameters corrected from the filtering effect may be found in Table 4.

simulated artificial planets in the data. We first removed the two planet solutions from the observed data, and we injected artificial planets of various masses corresponding to K amplitude ranging from 2 to 10 m s^{-1} with periods close, but not equal to, 3.7 days and 0.853 days. Then to simulate the whole process we ran the harmonic filtering to remove the activity, we adjusted the orbit, and we finally compared these results with the input values. No error was added to the radial velocity orbit to estimate the bias introduced by the filtering. For both periods we found that our process tends to underestimate the amplitude of the signal and this effect is stronger for the short period one. The correction is error-free, but depends a lot on the filtering parameter chosen. However, the amplitude of the planet solution is also affected by the time window considered. But together, the amplitude of the orbit corrected from the bias is constant, and therefore, independent of this parameter. With a coherence time of 20 days for a period around $P = 3.7$ days we found a 10% decrease in the amplitude, and for $P = 0.853$ days we found a 50% decrease in amplitude. In Table 4 both results (uncorrected and corrected) are listed.

As an additional check on our filtering process and of our results, we built a "simple" version of the harmonic filtering based on our Keplerian fitting tool with the radial velocity data sliced into 4 sets and treated separately. Actually this technique was first used to explore our ability to understand the complex structure of the radial velocity signal. We decided to include this analysis since it adds information on the robustness of our results. For each set we adjusted a Keplerian orbit on the most dominant of the first three rotation harmonic components (P_{rot}, $P_{\mathrm{rot}}/2$, $P_{\mathrm{rot}}/3$) and then removed it. Details on the sample selection of the analysis and solutions used to remove the most dominant rotation related activity term may be found in Table 5. Then the four "corrected" data sets were analyzed together.

In the power spectrum analysis of the filtered data, two peaks are clearly detected at 3.7 days and 5.8 days, the alias $\nu - 1$ of the CoRoT-7b transit period. Fixing $P = 0.8536$ d and Epoch $T_0 = 2\,454\,446.51$ and fitting a two-component circular Keplerian orbit, we found $K = 3.24 \pm 0.47$ m s^{-1} for the short period planet and $P = 3.666 \pm 0.006$ d, $K = 5.8 \pm 0.4$ m s^{-1} for the other planet. The solution found for CoRoT-7b is in full agreement with the other approaches. The amplitude of CoRoT-7c is 50% larger than the value found both by harmonic filtering

Table 4. Planetary solutions from radial velocity orbit fitting. See text for details.

Parameters	Solutions using filtering algorithm with the Pre-whitening	with the rotation harmonics	Adopted solution
	CoRoT-7b		
Period [days]	$0.85353 \pm 2 \times 10^{-5}$	0.8536 (fixed)	$0.853585 \pm 2.4 \times 10^{-5}$ (‡)
T_{tr} [JD]	2 454 446.7311 (fixed)	2 454 446.721 ± 0.028	2 454 446.731 ± 0.003 (‡)
T_0 [JD]		2 454 446.508 ± 0.029	
K [m s^{-1}]	(4.16 ± 0.27)† 3.33 ± 0.27 (±1)⋆	(1.9 ± 0.4)† 3.8 ± 0.8	3.5 ± 0.6
e	0.07 ± 0.067	0 (fixed)	0
ω [deg]	91.55 ± 49.27	180 (fixed)	180
m [$M_\oplus$]	4.5 ± 1	5.2 ± 1	4.8 ± 0.8
a [AU]			0.017
	CoRoT-7c		
Period [days]	3.701 ± 0.004	3.692 ± 0.008	3.698 ± 0.003
T_0 [JD]	2 454 445.34 ± 1.07	2 454 444.73 ± 0.87	2 454 445.0 ± 0.7
K [m s^{-1}]	(5.5 ± 0.3)† 4.4 ± 0.3 (±1)⋆	(3.5 ± 0.4)† 3.8 ± 0.5	4.0 ± 0.5
e	0.028 ± 0.048	0 (fixed)	0
ω [deg]	140 ± 98	180 (fixed)	180
m [$M_\oplus$]	9.4 ± 2.1 (*)	8.1 ± 0.9 (*)	8.4 ± 0.9
a [AU]			0.046
σ(O–C) [m s^{-1}]	1.81	2.82	
χ_{red}	1.2	1.3	

Notes: (†) Uncorrected amplitude solution from filtering effects. (⋆) Systematic error resulting from the filtering process. (‡) Adopted from Léger et al. (2009), (*) assuming CoRoT-7b and CoRoT-7c are on coplanar orbits ($\sin i = 80^0$).

Table 5. Data sets and their related parameters used for "simple" harmonic filtering processing (see text).

Sata sets start	Sata sets end	Duration (days)	Removed signal
54789	54807	18	circular solution with P_{rot}, $P_{rot}/2$
54825	54834	9	circular solution with $P_{rot}/3$
54847	54869	22	P_{rot}
54861	54884	23	circular solution P_{rot}, $P_{rot}/2$

of the data and the pre-whitening algorithm. We suspect that this could be a consequence of the data slicing and the correction of only the most dominant harmonics.

6. Discussing possible blend scenarios

In the many possible scenarios producing a faint transiting signal, there is the case of the hierarchical triple system with an eclipsing low-mass star or a faint eclipsing binary. These cases were discussed at length by Léger et al. (2009), who excluded an hierarchical triple system using the CoRoT color of the transit measurement and background unresolved binaries with additional high-contrast IR imaging. However, the authors point out that an unresolved K or M star companion orbited by a massive planet could not be excluded provided that its radial velocity is within 8 km s^{-1} of CoRoT-7. The detection of a radial velocity signal corresponding to the CoRoT-7b period puts a severe additional constraint on this alternative scenario. If one considers a background eclipsing system as an alternative scenario, it means that a fainter superimposed spectrum moves relative to the CoRoT-7 spectrum within a range of about km s^{-1} amplitude (from a hypothetical giant planet mass orbiting a background star). This scenario would correspond to a smaller scale version of the brown-dwarf orbiting the HD 41004 binary Santos et al. (2002). Therefore, similar to HD 41004, one would expect to see bisector span variations proportional to radial velocity variation.

It is obvious from Fig. 3 and the previous sections that the bisector variation is dominated by stellar activity with a slight global anti-correlation with the radial velocity. We decided to circumvent this problem by considering only bisector variations taken on the same night where a mean bisector and a mean radial velocity could be computed and differential "short term" values measured. In this way one builds a "differential" bisector span variation that is only sensitive to short-period variations. For each night with multiple observations, the typical longest offset between data is about 5 h, or about 25% of the phase variation. Obviously, by building a differential value, one increases the noise of each point. The outcome is a noisy diagram where theÊ bisector peak-to-peak variation is 20 m s^{-1} and the radial velocity range 10 m s^{-1}. By comparison with Fig. 3, activity is not detected. Actually, a positive slope of 0.45 ± 0.22 may be fit to the data. Spearman's rank test indicates a 2-σ deviation from the null correlation hypothesis. A bootstrap with 30 000 pools mixing radial velocity and bisectors also indicates a 2% probability that the correlation is just found by chance. Therefore we cannot exclude a linear relation between the radial velocity and the bisector on short-period while we can not demonstrate that it is related to the CoRoT-7b period.

To further exclude the possibility of a background transiting giant planet scenario, we decided to make the assumption that the slope of the bisector variations may indeed be related to the $P = 0.853$ d period. We simulated the effect of a background short-period giant planet on the bisector and the radial velocity signal of CoRoT-7. We explored a range of possible host star masses considering that 0.25 $M_\odot$ as the most massive star that could produce the observed transit signal, and 0.13 $M_\odot$ as the lightest one which would give a detectable effect on radial velocity. These two limits provide the range of possible contrasts for the background spectrum. A range of potential $v \sin i$ values for the background host stars has been considered, keeping in mind the possibility that the star may be synchronized with the orbiting planet thereby providing a upper value of 25 km s^{-1}. (For reference, a 1-day rotating M star with 0.3 $R_\odot$ would

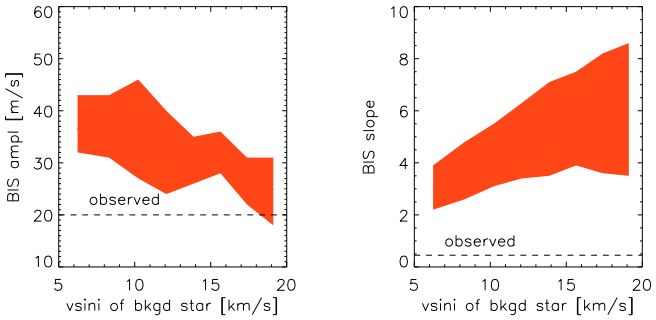

Fig. 12. Simulated amplitude (*left*) and slope (*right*) of the bisector span, which would be due to a binary blend, within limits imposed by observations. The horizontal axis shows the width of the simulated binary's cross-correlation function expressed in $v \sin i$ of the star. The filled zone shows the domain expected for the parameters, corresponding to various masses of the blend's primary from 0.25 to 0.1 $M_\odot$ and offset of 0 to 3 km s^{-1}. The dashed line indicates the upper limit derived from HARPS data (see in text).

correspond to about $v \sin i = 20$ km s^{-1}.) The results of our simulations are displayed in Fig. 12.

From the simulation, one finds that the slope of the relation of the bisector against the radial velocity is steeper than 2 in all cases. Actually the slope ranges from 2 to 6 depending on the ΔV_r between CoRoT-7 and the putative background star. The smallest slope is measured when $\Delta V_r = 3$ km s^{-1}. For larger offsets, the radial velocity variation deviates from the sine-curve description. The smallest bisector effect is measured for a $v \sin i = 25$ km s^{-1}broadened spectrum, whereas a bisector variation of 20 m s^{-1} amplitude would be expected. In conclusion, according to our model and our observed constraints on the bisector span slope (<1), a background star hosting a transiting giant planet can be excluded.

A power spectrum analysis of the bisector data does not detect any signal at the period of CoRoT-7c ($P = 3.7$ d). No evidence of a possible alternative origin of this period different from an orbiting planet is seen in the data.

7. Discussion

The radial velocity variability observed on CoRoT-7 is caused mainly by the activity in the photosphere of the star. This activity is strongly coupled to the rotation of the star and the presence of cool starspots in the atmosphere. A combined analysis of the spectroscopic and photometry data show various relations between the average spectroscopic parameters consistent with a rotating stellar surface having cool starspots. The level of activity of that star agrees with its estimated age between 1 and 2 Gyr. The overall activity of that star is fairly moderate by comparison with younger stars, but it is still a challenging limitation to overcome when trying to detect a planet in the super-Earth mass range with radial velocity measurements. Without the indication that a transit planet candidate was detected by CoRoT , it is very unlikely that we would have conducted such an intensive observation program with HARPS. The radial velocity survey for low-mass planets usually select their target stars based on their inactivity. Clearly, CoRoT-7 a G9 star between 1 and 2 Gyr age with 10 m s^{-1} rms intrinsic variability would have been excluded from the target list.

In our paper we used different approaches, and in all of them the CoRoT-7b period was detected in the radial velocity measurements, confirming that a stable and periodic physical phenomena produces this signal. The exact origin of the signal may, however, be debated. Instead of a real signal corresponding to the transit period of CoRoT-7b, an alternative solution would be to have a real 5.78 day periodic signal corresponding to the fourth harmonic of the rotation period ($P_{\rm rot}/4$) with its observed 1-day alias ($\nu + 1$) "by chance" matching exactly the CoRoT-7b transiting period. We believe that a body of evidence makes the 1-day alias interpretation very unlikely.

First, from the set of observed correlations between the photometry and the spectroscopic activity indicators, any harmonics of the rotation period should be seen both in spectroscopy and in photometry, similarly to the three first harmonics. In the FT of the CoRoT light curve (Fig. 7) no significant peak is detected at $P_{\rm rot}/4$. In addition the residuals of the harmonic decomposition of the *FWHM* of the CCF show no significant signal at $P_{\rm rot}/4$, it would be surprising that any correlation that would work for the first three harmonic would not be seen with the fourth one.

Second, from the radial velocity data alone, the 1-d alias is a rather far-fetched interpretation. Alias frequencies are generated by incomplete and sparse time coverage and they decrease with improved time sampling. The CoRoT-7b period is shorter than one day. Strictly speaking, given the sampling of the data, which is dominated by daily interruptions, we probably should be wary of any signal with a frequency above 1.0 c d^{-1} because it may merely be an alias of a low-frequency signal. However, real life is not that clear cut, since there are runs where we observed CoRoT-7 multiple times per night, so we expect the $\nu = 1.17$ d^{-1} and $\nu = 0.17$ d^{-1} to both be present in the radial velocity since these are aliases of each other (both ways). However, with the increase in the data sampling, the amplitude of the "alias peak" is expected to go away or at least to decrease. We simulated a sine-wave with $P = 5.68$ with 2 m s^{-1} white noise, sampled in the same way as the real data, and found that it would have an amplitude 6% higher than its short-period alias (at $\nu = 1.17$ c^{-1}). Actually the opposite is observed: the strongest signal is the short-period one. In the CLEAN analysis, the short-period peak is observed to be 5% stronger than the other one. Additionally when one fits the radial velocity data with a 3.6 d period planet and a sine-wave with $P = 5.68$ day, one finds that the amplitude of the $P = 5.68$ day signal is 30% weaker than with a short-period planet solution and a degradation of the fit quality. This result agrees with the Lomb Scargle analysis displayed in Fig. 10 where the $\nu = 0.17$ d^{-1} peak is not significant.

Perhaps the strongest arguments in favor of the CoRoT-7b planet origin of the observed signal is that the T_0 ephemerides of the planet solution agrees with the transit ephemerides of CoRoT-7b. This number scaled to the stellar photosphere would correspond to an active latitude located with 1.7^0 accuracy. Arguing in favor of the activity origin means considering that an active region has emerged precisely at the right place and holds its location on the stellar surface for the duration of the HARPS measurement. In statistical terms that is a 0.5% probability event. The orbiting transiting planet seems by far the simplest explanation.

A background eclipsing system scenario can be rejected from the many arguments given in Léger et al. (2009), as well our upper limit to any bisector variations. Considering the short distance between CoRoT-7b and its star, some time-dependent activity fluctuations on CoRoT-7 induced by the planet could be considered. Evidence suggesting a star-planet magnetic interaction between a star and its hot Jupiter as a cyclic variation of the stellar activity synchronized to the planets orbit has been observed (see for references in Shkolnik et al. 2009). Similar phenomena cannot be excluded, even for CoRoT-7b, while the planet is much smaller in our case. We looked for the signature

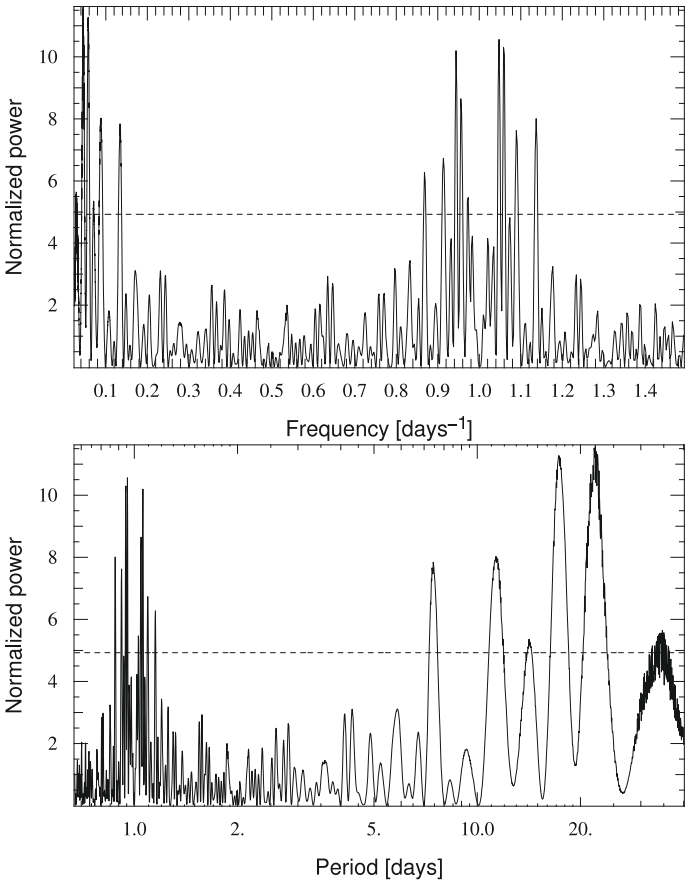

Fig. 13. Lomb Scargle periodogram analysis of the Ca H&K data. The hatched line indicates the 10^{-2} false alarm probability: *top*: expressed in unit of frequency; *bottom*: expressed in period unit.

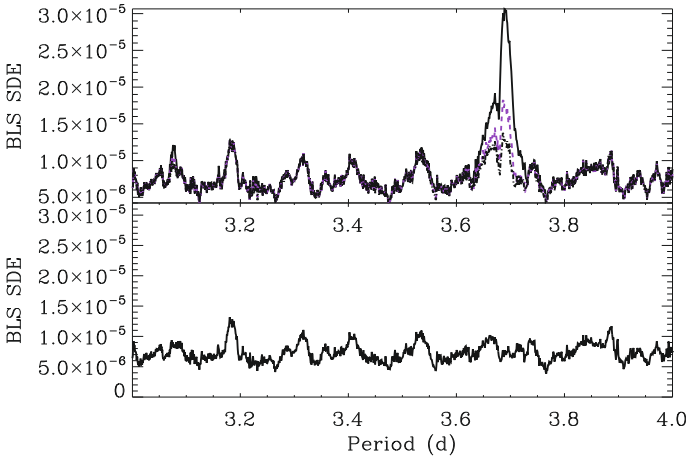

Fig. 14. Signal detection efficiency (SDE) of a search for additional planets in the CoRoT light curve in the period range between 3 and 4 days: *bottom*: result of the search in the original CoRoT light curve; *top*: same light curve with an additional simulated transiting planet at $P = 3.69$ day with 1.35, 0.95 and 0.6 $R_\oplus$.

of such interaction in the H&K Ca data. In the Lomb Scargle periodogram analysis, the two strongest peaks are found at the rotation period of CoRoT-7 and 17 days. No signal is detected at the CoRoT-7b period (see Fig. 13). Therefore we have no evidence that star-planet magnetic interaction between CoRoT-7 and its planet CoRoT-7b triggers a synchronized activity with the planet orbit.

The measurements presented in this paper firmly establish the planetary nature of the CoRoT-7b. The mass of CoRoT-7b is 4.8 $M_\oplus$. Combined with the radius estimates, an average mean density of the planet $\rho = 5.6 \pm 1.3\,\mathrm{g\,cm^{-3}}$, close to the Earth value $\rho_\oplus = 5.52\,\mathrm{g\,cm^{-3}}$, is computed, suggesting a rocky planet. However, CoRoT-7b is more massive than the Earth and the higher compression implies that it probably contains either less iron or more volatile materials (water, either as solid ice or as steam) (Seager et al. 2007; Valencia et al. 2007; Grasset et al. 2009). Detailed models of the planet (Valencia et al. 2009) indicate that it is consistent with a rocky planet made of silicates and an iron core of 0 to 30% of the total mass, or alternatively with a water-rich planet that could contain up to 40% of water as solid ice, or 10% water as steam.

From the point of view of its mass CoRoT-7b belongs to the category of "super-Earth" planets, lying between that of the Earth and Uranus. It is the first time that a density has been measured for such a small planet. Before CoRoT-7b, the smallest transiting planet known was GJ 436 (Gillon et al. 2007) with a measured density similar to Neptune. By comparison CoRoT-7b has a density almost three times higher. If one assumes that CoRoT-7b is representative of the "super Earth" population recently revealed by radial velocity surveys (Lovis et al. 2009), the structure of these planets is likely to be quite different from a Neptune-like structure.

The strongest periodic signal in the radial velocity data after removal of the activity is not CoRoT-7b but CoRoT-7c. Assuming both planets have orbital axes that are aligned, analogous to the planets in our Solar System, we get a mass of about 8 $M_\oplus$, placing CoRoT-7c in the mass range of the super-Earth planet category. The detection of a system of two short-period super-Earth mass planets is not surprising. Recent results from Doppler survey indicate that super-Earth mass planets rarely come alone, but instead in a system of planets (Mayor et al. 2009). It is interesting to note that the two orbital periods are in a 13/3 resonance, but that may be only a numerical coincidence. The detection of CoRoT-7c by transit timing variation (TTV) of CoRoT-7b transit is very unlikely. The expected TTV due to CoRoT-7c orbit is small because the system is not trapped in a strong resonance (like 1/2 for example). Moreover the effect of spots on the stellar atmosphere is likely to affect more the detail shape of transit ingress and egress measurements and produce larger variations.

The Hill-exclusion criteria is a convenient and robust proxy for estimating the stability of planetary systems (Hayes & Tremaine 1998). In the present context of low-mass, close-in compact systems they can be simply expressed as a minimum relative period separation $\Delta P/P$ for two equal mass neighboring planets of mass m in orbit around the star of mass M (Funk et al. 2009):

$$\frac{\Delta P}{P} = 3^{2/3} k \left(\frac{m}{M}\right)^{\frac{1}{3}}, \quad (1)$$

with $k \sim 4$ for two planet geometry (Smith & Lissauer 2009). With the mass m of CoRoT-7c one finds $\Delta P/P > 0.6$. That is easily satisfied by the orbital configuration shown in Table 4.

We searched for the transit signal of CoRoT-7c in the CoRoT light curve. We first removed the best-fit model of CoRoT-7b from the filtered CoRoT-7 light curve and performed a standard BLS (Kovács et al. 2002) search for transit signals with periods between 3 and 4 days. To establish the detectability of a few $R_\oplus$ transiting object at this period, we constructed several light curves with simulated transits of different depths, corresponding to radii between 0.6 and 1.35 $R_\oplus$. The resulting signal detection efficiencies (SDE) for the simulated and the original

curves are displayed in Fig. 14. We can safely conclude from that figure that transiting objects with radii larger than 1.4 $R_\oplus$ would have been clearly detected in the data. As the expected radius of an 8 $M_\oplus$ object is above 1.8 $R_\oplus$, the most reasonable assumption is that the planet CoRoT-7c is not transiting. Assuming a circular orbit and taking the stellar parameters from Léger et al. (2009), the inclination of CoRoT-7c should then be less than 85 deg to agree with its semi-major axis and the lack of transit. This value does not exclude the possibility of near coplanar orbits, since the best-fit inclination of CoRoT-7b is 80 ± 0.3 deg (Léger et al. 2009).

CoRoT-7 is the first star discovered with a planetary system made of two short-period super-Earth mass planets with one in transit. This system illustrates the potential of precise radial velocity follow-up of a transiting planet, underlying as well the difficulties related to the activity of stars of intermediate ages and the extraction of planetary orbital perturbation signatures. CoRoT-7 is one of the brightest stars with a transiting planet. Extrapolating our result to planets producing weaker Doppler effects, we either need to use a bigger telescope or search for small transiting planets around brighter stars. These two main avenues for future research are addressed by the main science drivers of the ESPRESSO spectrograph for the VLT (Pasquini et al. 2009) and ongoing study of the PLATO space transit search mission (Fridlund 2009).

Acknowledgements. The authors thank the many observers who contributed to the intensive observation campaign of CoRoT-7, and Suzanne Agrain for useful comments and discussions on the manuscript. In particular we thank our referee, Gordon Walker, for his fast response and his useful comments that have improved the paper. We are grateful to all the staff of La Silla Observatory for their contribution to the success of the HARPS project and operation. The German CoRoT Team (TLS and Univ. Cologne) acknowledges DLR grants 50OW0204, 50OW0603, 50QP07011. The team at IAC acknowledges support by grant ESP2007-65480-C02-02 of the Spanish Ministerio de Ciencia e Inovación. The French team wish to thank the "Programme National de Planétologie" (PNP) of CNRS/INSU and the French National Research Agency (ANR-08-JCJC-0102-01) for their continuous support to our planet-search programs. The Swiss team acknowledges the ESA PRODEX program and the Swiss National Science Foundation for their continuous support on CoRoT ground follow-up.

References

Boisse, I., Moutou, C., Vidal-Madjar, A., et al. 2009, A&A, 495, 959
Bouchy, F., & Queloz, D. 2007, Transiting Extrapolar Planets Workshop, 366, 193
Bouchy, F., Moutou, C., Queloz, D., & the CoRoT Exoplanet Science Team 2009, IAU Symp., 253, 129
Breger, M., & Pamyatnykh, A. A. 2006, MNRAS, 368, 571
Castenmiller, M. J. M., Zwaan, C., & van der Zalm, E. B. J. 1986, Sol. Phys., 105, 237
Deeg, H. J., Gillon, M., Shporer, A., et al. 2009, A&A, 506, 343
Donahue, R. A., Dobson, A. K., & Baliunas, S. L. 1997, Sol. Phys., 171, 191
Edelson, R. A., & Krolik, J. H. 1988, ApJ, 333, 646
Fridlund, M. 2009, IAU Symp., 253, 564
Funk, et al. 2009, A&A, submitted
Gillon, M., Pont, F., Demory, B.-O., et al. 2007, A&A, 472, L13
Grasset, O., Schneider, J., & Sotin, C. 2009, ApJ, 693, 722
Hayes, W., & Tremaine, S. 1998, Icarus, 135, 549
Hebb, L., Collier-Cameron, A., Loeillet, B., et al. 2009, ApJ, 693, 1920
Kovács, G., Zucker, S., & Mazeh, T. 2002, A&A, 391, 369
Kuschnig, R., Weiss, W. W., Gruber, R., Bely, P. Y., & Jenkner, H. 1997, A&A, 328, 544
Léger, A., Rouan, D., Schneider, et al. 2009, A&A, 506, 287
Lenz, P., & Breger, M. 2004, The A-Star Puzzle, 224, 786
Lovis, C., Mayor, M., Bouchy, F., et al. 2009, IAU Symp., 253, 502
Mayor, M., Pepe, F., Queloz, D., et al. 2003, Msngr., 114, 20
Mayor, M., Udry, S., Lovis, C., et al. 2009, A&A, 493, 639
Mazeh, T., Naef, D., Torres, G., et al. 2000, ApJ, 532, L55
Melo, C., Santos, N. C., Gieren, W., et al. 2007, A&A, 467, 721
Noyes, R. W., Weiss, N. O., & Vaughan, A. H. 1984, ApJ, 287, 769
Pasquini, L., et al. 2009, Science with the VLT in the ELT Era, 395
Queloz, D. 1999, NATO ASIC Proc. 532: Planets Outside the Solar System: Theory and Observations, 229
Queloz, D., Henry, G. W., Sivan, J. P., et al. 2001, A&A, 379, 279
Saar, S. H., & Donahue, R. A. 1997, ApJ, 485, 319
Saar, S. H., Butler, R. P., & Marcy, G. W. 1998, ApJ, 498, L153
Santos, N. C., Mayor, M., Naef, D., et al. 2000, A&A, 361, 265
Santos, M., Mayor, D., Naef, D., et al. 2002, A&A, 392, 215
Seager, S., Kuchner, M., Hier-Majumder, C. A., & Militzer, B. 2007, ApJ, 669, 1279
Shkolnik, E., Aigrain, S., Cranmer, S., et al. 2009, AIP Conf. Ser., 1094, 275
Smith, A. W., & Lissauer, J. J. 2009, Icarus, 201, 381
Torres, G., Konacki, M., Sasselov, D. D., & Jha, S. 2004, ApJ, 614, 979
Valencia, D., Sasselov, D. D., & O'Connell, R. J. 2007, ApJ, 665, 1413
Valencia, D., Ikoma, M., Guillot, T., & Nettelmann, N. 2009, A&A, submitted [arXiv:0907.3067]
White, R. J., & Peterson, B. M. 1994, PASP, 106, 879

[1] Observatoire de Genève, Université de Genève, 51 Ch. des Maillettes, 1290 Sauverny, Switzerland
e-mail: didier.queloz@unige.ch
[2] Institut d'Astrophysique de Paris, UMR7095 CNRS, Université Pierre & Marie Curie, 98bis Bd Arago, 75014 Paris, France
[3] Observatoire de Haute-Provence, CNRS/OAMP, 04870 St Michel l'Observatoire, France
[4] Laboratoire d'Astrophysique de Marseille, UMR 6110, Technopole de Marseille-Étoile, 13388 Marseille Cedex 13, France
[5] Thüringer Landessternwarte Tautenburg, Sternwarte 5, 07778 Tautenburg, Germany
[6] LESIA, CNRS UMR 8109, Observatoire de Paris, 5 place J. Janssen, 92195 Meudon, France
[7] Physikalisches Insitut, University of Bern, Sidlerstrasse 5, 3012 Bern, Switzerland
[8] IAS, UMR 8617 CNRS, bat 121, Université Paris-Sud, 91405 Orsay, France
[9] Instituto de Astrofísica de Canarias, E-38205 La Laguna, Spain
[10] Institute for Astronomy, University of Vienna, Türkenschanzstrasse 17, 1180 Vienna, Austria
[11] Institute of Planetary Research, DLR, Rutherfordstr. 2, 12489 Berlin, Germany
[12] IAG-Universidade de Sao Paulo, Brazil
[13] Research and Scientific Support Department, European Space Agency, ESTEC, 2200 Noordwijk, The Netherlands
[14] Institut d'Astrophysique et de Géophysique, Université de Liège, Allée du 6 août 17, Sart Tilman, Liège 1, Belgium
[15] Observatoire de la Côte d'Azur, Laboratoire Cassiopée, CNRS UMR 6202, BP 4229, 06304 Nice Cedex 4, France
[16] Space Research Institute, Austrian Academy of Sciences, Schmiedlstrasse 6, 8042 Graz, Austria
[17] School of Physics and Astronomy, R. and B. Sackler Faculty of Exact Sciences, Tel Aviv University, Tel Aviv 69978, Israel
[18] Rheinisches Institut für Umweltforschung, Universität zu Köln, Abt. Planetenforschung, Aachener Str. 209, 50931 Köln, Germany
[19] Center for Astronomy and Astrophysics, TU Berlin, Hardenbergstr. 36, 10623 Berlin, Germany
[20] LUTH, Observatoire de Paris-Meudon, 5 place J. Janssen, 92195 Meudon, France

Pages 318 and 319 (Appendix A) are available in the electronic edition of the journal at http://www.aanda.org

Appendix A

Table A.1. HARPS data used in this paper.

JDB (–2400000.0)	v_{rad} (km s^{-1})	$\sigma(v_{rad})$ (km s^{-1})	*FWHM* (km s^{-1})	σ(*FWHM*) (km s^{-1})	span (km s^{-1})	σ(span) (km s^{-1})	log(R'(HK))	σ(log(R'(HK)))
54527.543878	31.1818	0.0015	6.4648	0.0035	0.0258	0.0030	–4.6646	0.0059
54530.604318	31.1732	0.0015	6.4666	0.0035	0.0309	0.0030	–4.6736	0.0063
54550.503296	31.1972	0.0021	6.4621	0.0049	0.0191	0.0042	–4.6269	0.0116
54775.819119	31.1881	0.0022	6.5028	0.0052	0.0340	0.0044	–4.5847	0.0103
54776.758450	31.1848	0.0028	6.4981	0.0066	0.0317	0.0056	–4.5702	0.0151
54777.761675	31.1817	0.0020	6.4993	0.0047	0.0400	0.0040	–4.6251	0.0102
54778.754586	31.1734	0.0016	6.4875	0.0038	0.0241	0.0032	–4.5877	0.0071
54779.750679	31.1750	0.0022	6.4969	0.0052	0.0252	0.0044	–4.6391	0.0117
54780.754792	31.1805	0.0026	6.4915	0.0061	0.0278	0.0052	–4.5494	0.0128
54789.829872	31.1878	0.0016	6.5050	0.0038	0.0235	0.0032	–4.6037	0.0068
54790.802989	31.1914	0.0021	6.5096	0.0049	0.0148	0.0042	–4.6447	0.0117
54791.810991	31.1990	0.0019	6.5131	0.0045	0.0214	0.0038	–4.5960	0.0087
54792.809988	31.1933	0.0018	6.5316	0.0042	0.0264	0.0036	–4.6105	0.0083
54793.827734	31.1855	0.0018	6.5291	0.0042	0.0225	0.0036	–4.5999	0.0078
54794.800626	31.1901	0.0017	6.5329	0.0040	0.0309	0.0034	–4.5987	0.0074
54795.809029	31.1835	0.0022	6.5225	0.0052	0.0231	0.0044	–4.5687	0.0101
54796.836494	31.1756	0.0017	6.5295	0.0040	0.0210	0.0034	–4.5706	0.0069
54797.803411	31.1787	0.0017	6.5220	0.0040	0.0336	0.0034	–4.5931	0.0069
54798.806092	31.1925	0.0025	6.5168	0.0059	0.0379	0.0050	–4.6300	0.0145
54799.776987	31.1926	0.0019	6.5064	0.0045	0.0278	0.0038	–4.6129	0.0091
54799.864538	31.1977	0.0025	6.4690	0.0059	0.0278	0.0050	–4.6267	0.0142
54800.759086	31.1880	0.0021	6.4832	0.0049	0.0379	0.0042	–4.5987	0.0104
54800.846162	31.1857	0.0016	6.4987	0.0038	0.0362	0.0032	–4.5825	0.0067
54801.753036	31.1832	0.0015	6.4882	0.0035	0.0353	0.0030	–4.6097	0.0062
54801.839649	31.1851	0.0015	6.4922	0.0035	0.0392	0.0030	–4.6100	0.0065
54802.748385	31.1854	0.0020	6.4764	0.0047	0.0216	0.0040	–4.6389	0.0108
54802.843308	31.1835	0.0016	6.4793	0.0038	0.0328	0.0032	–4.6340	0.0073
54803.752610	31.1815	0.0018	6.4812	0.0042	0.0292	0.0036	–4.6480	0.0093
54803.834177	31.1789	0.0020	6.4811	0.0047	0.0194	0.0040	–4.6384	0.0111
54804.755468	31.1782	0.0025	6.4783	0.0059	0.0187	0.0050	–4.6712	0.0153
54804.834245	31.1847	0.0019	6.4894	0.0045	0.0246	0.0038	–4.6637	0.0104
54805.777470	31.1970	0.0021	6.4914	0.0049	0.0115	0.0042	–4.6622	0.0116
54805.850494	31.2039	0.0024	6.4902	0.0056	0.0202	0.0048	–4.6645	0.0145
54806.764734	31.2044	0.0018	6.4970	0.0042	0.0211	0.0036	–4.6659	0.0098
54806.844413	31.2036	0.0022	6.5003	0.0052	0.0187	0.0044	–4.5884	0.0112
54807.728119	31.1937	0.0018	6.5033	0.0042	0.0230	0.0036	–4.6484	0.0087
54807.826352	31.1965	0.0017	6.5042	0.0040	0.0215	0.0034	–4.6372	0.0084
54825.736813	31.1916	0.0013	6.4712	0.0031	0.0241	0.0026	–4.6173	0.0053
54826.739453	31.1943	0.0014	6.4814	0.0033	0.0154	0.0028	–4.6372	0.0056
54827.726165	31.2018	0.0014	6.4919	0.0033	0.0145	0.0028	–4.6300	0.0055
54828.736070	31.2160	0.0017	6.5082	0.0040	0.0136	0.0034	–4.6462	0.0082
54829.735395	31.2057	0.0020	6.5080	0.0047	0.0203	0.0040	–4.5906	0.0094
54830.724394	31.1881	0.0018	6.5219	0.0042	0.0333	0.0036	–4.5798	0.0072
54831.710289	31.1788	0.0066	6.4794	0.0155	0.0314	0.0132	–4.7112	0.0559
54831.728761	31.1753	0.0019	6.5141	0.0045	0.0229	0.0038	–4.5731	0.0079
54832.725234	31.1865	0.0030	6.5149	0.0070	0.0270	0.0060	–4.5826	0.0154
54833.734170	31.1892	0.0021	6.5046	0.0049	0.0263	0.0042	–4.6322	0.0101
54834.753950	31.2003	0.0015	6.5311	0.0035	0.0256	0.0030	–4.6106	0.0064
54847.596797	31.1890	0.0017	6.4744	0.0040	0.0290	0.0034	–4.6204	0.0076
54847.693890	31.1908	0.0018	6.4815	0.0042	0.0364	0.0036	–4.6069	0.0078
54847.756817	31.1909	0.0015	6.4918	0.0035	0.0365	0.0030	–4.6376	0.0068
54848.600709	31.1846	0.0015	6.4631	0.0035	0.0240	0.0030	–4.6154	0.0060
54848.682235	31.1792	0.0013	6.4774	0.0031	0.0339	0.0026	–4.6198	0.0051
54848.759062	31.1758	0.0016	6.4780	0.0038	0.0253	0.0032	–4.6320	0.0073
54849.594019	31.1835	0.0014	6.4840	0.0033	0.0271	0.0028	–4.6309	0.0056
54849.671887	31.1786	0.0015	6.4729	0.0035	0.0189	0.0030	–4.5915	0.0061
54849.749061	31.1791	0.0019	6.4766	0.0045	0.0106	0.0038	–4.6242	0.0099
54850.595162	31.1869	0.0018	6.4818	0.0042	0.0178	0.0036	–4.6317	0.0086
54850.664176	31.1878	0.0016	6.4844	0.0038	0.0344	0.0032	–4.6297	0.0073
54850.750354	31.1907	0.0014	6.4824	0.0033	0.0250	0.0028	–4.6218	0.0059
54851.592681	31.1914	0.0017	6.4799	0.0040	0.0255	0.0034	–4.6292	0.0081
54851.666440	31.1926	0.0018	6.4860	0.0042	0.0215	0.0036	–4.6356	0.0082

Table A.1. continued.

JDB (–2400000.0)	$v_{\rm rad}$ (km s^{-1})	$\sigma(v_{\rm rad})$ (km s^{-1})	$FWHM$ (km s^{-1})	$\sigma(FWHM)$ (km s^{-1})	span (km s^{-1})	σ(span) (km s^{-1})	log(R'(HK))	σ(log(R'(HK)))
54851.747584	31.1923	0.0018	6.4896	0.0042	0.0299	0.0036	–4.6370	0.0092
54852.598578	31.1892	0.0018	6.4905	0.0042	0.0300	0.0036	–4.6242	0.0086
54852.673969	31.1861	0.0015	6.4851	0.0035	0.0182	0.0030	–4.6349	0.0064
54852.741247	31.1918	0.0016	6.4858	0.0038	0.0298	0.0032	–4.6192	0.0070
54853.573953	31.1961	0.0015	6.4996	0.0035	0.0314	0.0030	–4.6002	0.0061
54853.698128	31.2004	0.0015	6.4863	0.0035	0.0266	0.0030	–4.5767	0.0062
54853.746135	31.2008	0.0016	6.5049	0.0038	0.0188	0.0032	–4.6006	0.0075
54854.580252	31.2062	0.0017	6.4841	0.0040	0.0247	0.0034	–4.5825	0.0071
54854.657842	31.2074	0.0016	6.4938	0.0038	0.0265	0.0032	–4.6009	0.0070
54854.741682	31.2001	0.0019	6.4990	0.0045	0.0204	0.0038	–4.6045	0.0090
54855.675459	31.2003	0.0014	6.5085	0.0033	0.0198	0.0028	–	–
54856.652751	31.1942	0.0013	6.5201	0.0031	0.0228	0.0026	–	–
54857.646823	31.2091	0.0013	6.5261	0.0031	0.0157	0.0026	–	–
54858.663463	31.2130	0.0019	6.5245	0.0045	0.0214	0.0038	–	–
54859.649883	31.2013	0.0022	6.5382	0.0052	0.0265	0.0044	–	–
54860.752152	31.1907	0.0060	6.5464	0.0141	0.0274	0.0120	–	–
54861.684451	31.1991	0.0014	6.5384	0.0033	0.0387	0.0028	–	–
54862.662718	31.1898	0.0021	6.5269	0.0049	0.0297	0.0042	-	–
54863.655034	31.1784	0.0015	6.5313	0.0035	0.0299	0.0030	–	–
54864.630186	31.1747	0.0056	6.5221	0.0132	0.0325	0.0112	–4.5171	0.0293
54865.597778	31.1871	0.0027	6.5024	0.0063	0.0279	0.0054	–4.6057	0.0122
54865.715909	31.1829	0.0020	6.4980	0.0047	0.0347	0.0040	–4.5831	0.0081
54866.660215	31.1768	0.0027	6.5042	0.0063	0.0409	0.0054	–4.5755	0.0125
54867.560377	31.1633	0.0022	6.4961	0.0052	0.0366	0.0044	–4.6310	0.0101
54867.670638	31.1646	0.0022	6.4985	0.0052	0.0333	0.0044	–4.5947	0.0100
54868.591829	31.1675	0.0024	6.4874	0.0056	0.0197	0.0048	–4.5811	0.0100
54868.687553	31.1695	0.0028	6.4775	0.0066	0.0241	0.0056	–4.5895	0.0135
54869.600213	31.1848	0.0016	6.4819	0.0038	0.0328	0.0032	–4.6305	0.0059
54869.688032	31.1890	0.0017	6.4881	0.0040	0.0304	0.0034	–4.6193	0.0071
54870.601258	31.1868	0.0016	6.4943	0.0038	0.0260	0.0032	–4.6314	0.0063
54870.715742	31.1872	0.0021	6.4859	0.0049	0.0203	0.0042	–4.6203	0.0095
54871.537976	31.1923	0.0015	6.4816	0.0035	0.0198	0.0030	–4.6192	0.0060
54872.564758	31.2030	0.0023	6.4747	0.0054	0.0320	0.0046	–4.6300	0.0116
54872.649638	31.1980	0.0017	6.4778	0.0040	0.0282	0.0034	–4.6626	0.0077
54872.727318	31.1928	0.0023	6.4755	0.0054	0.0211	0.0046	–4.6382	0.0125
54873.537549	31.1950	0.0022	6.4752	0.0052	0.0226	0.0044	–4.6433	0.0111
54873.650147	31.1929	0.0015	6.4829	0.0035	0.0115	0.0030	–4.6436	0.0068
54873.720073	31.1902	0.0020	6.4774	0.0047	0.0270	0.0040	–4.6511	0.0108
54879.536551	31.2017	0.0020	6.4994	0.0047	0.0268	0.0040	–4.6174	0.0094
54879.676148	31.1990	0.0022	6.4929	0.0052	0.0310	0.0044	–4.5864	0.0109
54880.613748	31.2054	0.0022	6.5075	0.0052	0.0337	0.0044	–4.6504	0.0121
54881.591054	31.2038	0.0017	6.5156	0.0040	0.0181	0.0034	–4.6057	0.0075
54882.525655	31.1987	0.0016	6.5294	0.0038	0.0247	0.0032	–4.6045	0.0068
54882.656016	31.2034	0.0016	6.5303	0.0038	0.0244	0.0032	–4.5665	0.0067
54883.588012	31.2043	0.0015	6.5263	0.0035	0.0187	0.0030	–4.5945	0.0060
54884.526256	31.1985	0.0016	6.5235	0.0038	0.0319	0.0032	–4.5841	0.0063
54884.646409	31.1903	0.0020	6.5209	0.0047	0.0304	0.0040	–4.5816	0.0093